



Synergistic hollow CoMo oxide dual catalysis for tandem oxygen transfer: Preferred aerobic epoxidation of cyclohexene to 1,2-epoxycyclohexane

Wenzhou Zhong, Mengqiao Liu, Jing Dai, Jian Yang, Liqiu Mao, Dulin Yin*

National & Local United Engineering Laboratory for New Petrochemical Materials & Fine Utilization of Resources, Hunan Normal University, Changsha 410081, PR China



ARTICLE INFO

Keywords:

Cyclohexene
1,2-Epoxyhexane
CoMo oxide
Synergistic catalysis
Molecular oxygen

ABSTRACT

The CoMo hollow bimetallic oxide has been exploited in the aerobic epoxidation of cyclohexene containing labile allylic hydrogen atoms using ethylbenzene as a solvent. Cooperativity between Co(II) and Mo(VI) sites consisting of Co—O—Mo or Mo—O^{δ−}...Co^{δ+} unit on hollow oxide surfaces is investigated for controlling preferred epoxidation catalysis via tandem oxygen transfer. Various characterization techniques like XRD diffraction, N₂ physisorption, TEM, and Raman, XPS, Infrared, and UV-vis spectroscopies are employed to reveal the relationship between structure of active sites and catalytic performance. Together with these comprehensive experimental and computational studies, in this unique tandem catalytic process, Co(II) sites effectively mediate the first step of the overall oxidation cycle yielding a phenylethylperoxy radical by oxygen activation [Co(II) to Co(III)—O₂[−] to phenylethyl radical and finally to a phenylethylperoxy radical]. On the other hand, Mo(VI) sites are shown to be the excellent catalytic species for the subsequent epoxidation step by the transfer of oxygen atom of the phenylethylperoxy radical to cyclohexene. Hence, a 59% epoxidation selectivity with 33% cyclohexene conversion is accomplished through the required combination of Co(II) and Mo(VI) (2:1), allowing to tune epoxidation efficiency toward higher driving forces (relative to oxygenation of allylic hydrogen atom). This remarkably different catalytic performances between Co(II) and Mo(VI) can be attributed to the stronger overall polarization ability of Mo(VI) toward σ* O—O orbital of the O—O unit derived from its d-type orbitals, which helps the donor-acceptor interactions with the double bond.

1. Introduction

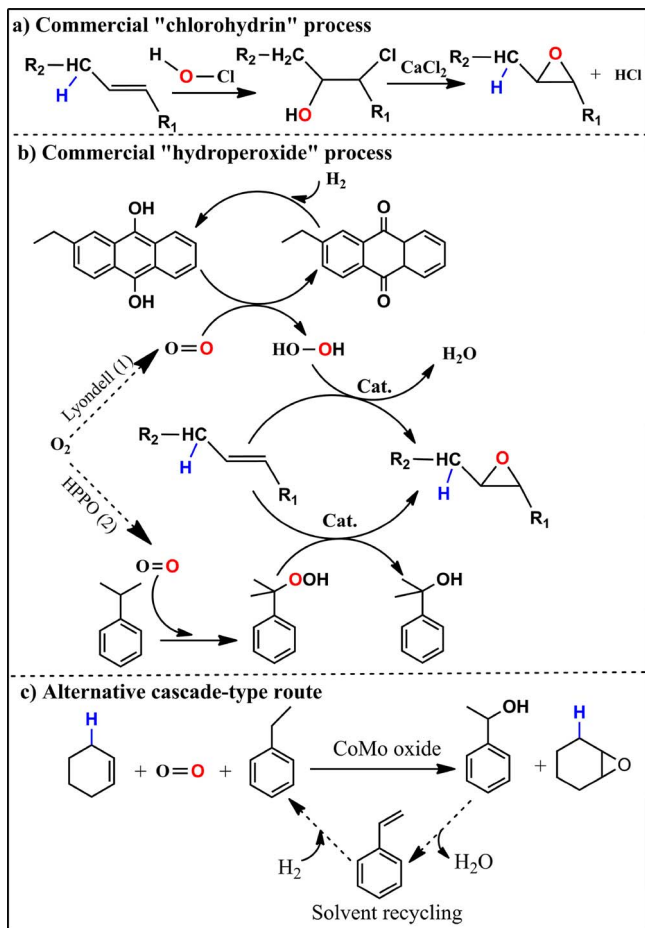
Selective oxidation is of critical importance to fundamental and applied research, remaining a key challenge in large-scale industrial processes that convert hydrocarbons into higher-value chemical feedstocks [1]. Invariably molecular oxygen from the air is considered to be a waste-free and abundant oxidant of choice, which has been desired in view of green chemistry [2]. One of the greatest interests in the field of oxidation chemistry is the electrophilic additions of O₂ to alkenes to yield epoxides [3]. Since molecular oxygen lies a stable paramagnetic structure (with two unpaired electrons in ground state); therefore, its reaction with alkene being diamagnetic, is usually spin-forbidden. Although there is a rare exception limited to gas phase capable of achieving this goal for the ethylene or propene epoxidation on a very large scale, extension of this chemistry to the efficient epoxidation of cyclohexene with containing labile allylic hydrogen atoms is a challenging unsolved problem. Apparently, the major obstacle to directly epoxidize higher cyclohexene with containing labile allylic hydrogen atoms can be related to the fact that the dissociation energy of the

allylic C—H bond in higher cyclohexene is ~77 kcal/mol while the corresponding dissociation energy of the vinylic C—H bond in ethylene is much larger (~112 kcal/mol). Thus, facile allylic C—H bond cleavage in cyclohexene by molecular oxygen commonly results in a low epoxidation selectivity. Current worldwide epoxide production still relies on the “chlorohydrin” process (Dow) with aqueous solution of alkalis [4] and “hydroperoxide” process (Lyondell, Shell, Sumitomo, and Repsol) [5,6], as depicted in Scheme 1. The former method consumes large amounts of chlorine, yielding an equimolar quantity of waste aqueous solution of alkali metal chlorides. The latter method involves peroxide-oxidants such as H₂O₂, cumene hydroperoxide, ethylbenzene hydroperoxide, and *tert*-butyl hydroperoxide, which is often expensive and tend to be hazardous to handle.

In the “hydroperoxide” process, there is a general mechanistic feature of these synthetic methods proceeding by way of the electrophilic addition of oxygen-centered radicals to alkenes. The oxygen-centered radicals from alkyl hydroperoxide or H₂O₂ (which is an active oxygen carrier) is considered to be attained through use of alkane or H₂ where sacrificial reducing agents and coreactants, supply the energy for the

* Corresponding author.

E-mail address: dulinyin@126.com (D. Yin).



Scheme 1. Existing commercial route (a) and (b) and alternative cascade-type reaction (c) for cyclohexene epoxidation.

scission of the O–O bond of O₂ that leads to formation of alcohol and H₂O (**Scheme 1**). Namely, the application of one oxygen atom of O₂ with symmetric structure leaves behind the other atom that needs protons and electrons to yield a stable compound. This process is very similar to the activation of O₂ in the “biological world” for alkene epoxidation by the use of monooxygenase-type enzyme as an oxygen transfer molecule [7]. In this context, many intriguing oxygen-activation systems have been investigated by the aerobic epoxidation of alkenes combined with a sacrificial reducing agents, e.g., O₂/H₂ [8], O₂/Zn [9], or an O₂/organic reductant (prominently aldehyde or alcohol) [10]. Despite excellent selectivity, the reaction rates apparently are too low, as well as the need of a large excess of reductant for synthetically reasonable application. Recently, the use of heterogeneous catalysts such as Co-modified zeolite [11] and FePt@Cu nanowires [12], well known for direct stilbene epoxidation with O₂, can not be extended to substrates that contains labile allylic H atoms.

Transition-metal cobalt catalysts are well-known to catalyze the selective oxidation of alkanes and alkylbenzenes efficiently to organic oxygenates by O₂ [13]. It has been noted that transition-metal cobalt(II) sites can bind and activate oxygen to form Co(III)–O^{−2} species, which further undergo reaction to yield peroxy or superoxo radical-type active oxygens. However, only a few examples of catalytic epoxidation of alkenes using cobalt catalysts have surfaced in the literature [11,14,15]. Commonly encountered complications include a limited substrate scope (stilbene), use of organic reductant, and/or low selectivities with main byproducts resulting from allylic C–H bond cleavage frequently observed. For example, CoCl₂ was investigated for the aerobic oxidation of monoterpenes, and in this case allylic oxidation proceeded predominantly [14]. Cobalt salen complexes were reported to show

catalytic activity for aerobic epoxidation of styrene in the presence of a co-reductant, isobutyraldehyde [15]. Recently, Beier et al. used the cobalt(II)-exchanged zeolite modified by alkali metal, which shows high activity in the aerobic epoxidation of stilbene without the need for a co-reductant [11]. They proposed an alternative explanation of epoxidation on the basis of a higher stabilization of activate oxygen intermediate by the active phase with alkaline earth cation. As a result, an emerging approach to enhance catalytic performance of the catalysts for alkene epoxidation is to couple the second metal with favored electronic effects.

In this sense, transition-metal molybdenum-based catalysts have proven to be highly active and selective in the aerobic epoxidation with alkyl hydroperoxides as oxygen sources [16]. The large positive charge of the Mo metals is capable of accepting electron pairs in vacant d orbitals, leading to the formation of stable complexes with alkyl hydroperoxides. Moreover, this formation process causes the peroxidic distal O atom to be more electrophilic and, therefore, more likely to be attacked by an olefinic C=C bond [17]. For example, the MoBr₂(O)₂-(NCC₆H₅)₂ complexes have been reported to accomplish the epoxidation of *cis*-cyclooctene in a 65% yield [18]. The complex dichlorodioxomolybdenum coordinated by the 2, 2-di(1-pyrazolyl)-propane ligand has been investigated, and showed a moderate catalytic reactivity with a 100% yield at 24 h reaction time [19]. However, these catalysts are not very stable and they easily decompose during the course of the reaction.

Thus, it appears to us that it should be possible to design an efficient direct process in which the two reaction steps, i.e. the formation of the peroxide and epoxidation of alkene containing labile allylic hydrogen atoms, will occur concurrently in a cascade-type reaction. Meanwhile, solvent can be regenerated by dehydration and hydrogenation process, which is satisfied with the requirement of green chemistry (**Scheme 1c**). Inspired by the dual activation of O₂ and cyclohexene epoxidation by the above overviewed Co and Mo-based catalyst systems, we envisioned that a combination of the less positive charge metal cobalt site, which could be sufficiently potent to render ethylbenzene fixation into ethylbenzene peroxide (EBHP), with the more positive charge Mo, which favors EBHP activation for subsequent steps of epoxidation, could serve as a tandem system that effectively converts cyclohexene to epoxide. The cooperativity between Co(II) and Mo(VI) sites consisting of Co–O–Mo or Mo–O^{δ−}...Co^{δ+} unit on oxide surfaces should allow us to develop more economical, efficient, and recyclable tandem epoxidation catalysts based on an interior active oxygen carrier platform. Accordingly, investigations of hollow CoMo bimetallic oxide can be helpful for better understanding details of oxygen transfer reactions, which, when each used only, is ineffective for catalyzing direct epoxidation of alkenes such as cyclohexene. Herein, we present a full account of our combined experimental and theoretical investigations into this novel tunability of CoMo bimetallic oxide for oxygen transfer reaction.

2. Experimental

2.1. Catalyst preparation

The hollow CoMo bimetallic oxides were prepared via a facile co-precipitation method reported in Ref. [20]. Typically, Co(NO₃)₂·6H₂O (2.91 g) and (NH₄)₆Mo₇O₂₄·4H₂O (0.883 g) were separately dissolved into 100 mL of distilled water at room temperature, resulting in a clear red solution. Then 5 mL of ammonium hydroxide solution was added to the above solution dropwise under stirring, and the final pH was controlled to ca. 6.5. Afterward, the resultant solution was heated to 85 °C in a hot bath. During this process, once part of the water had evaporated a purple precipitate formed. The obtained slurry was then dried at 100 °C overnight, and calcined at 500 °C for 5 h in air to obtain the final product. The hollow CoMo oxide catalysts having various Co/Mo ratios (namely 1:3, 1:2, 1:1, 1:3) were prepared by an identical procedure

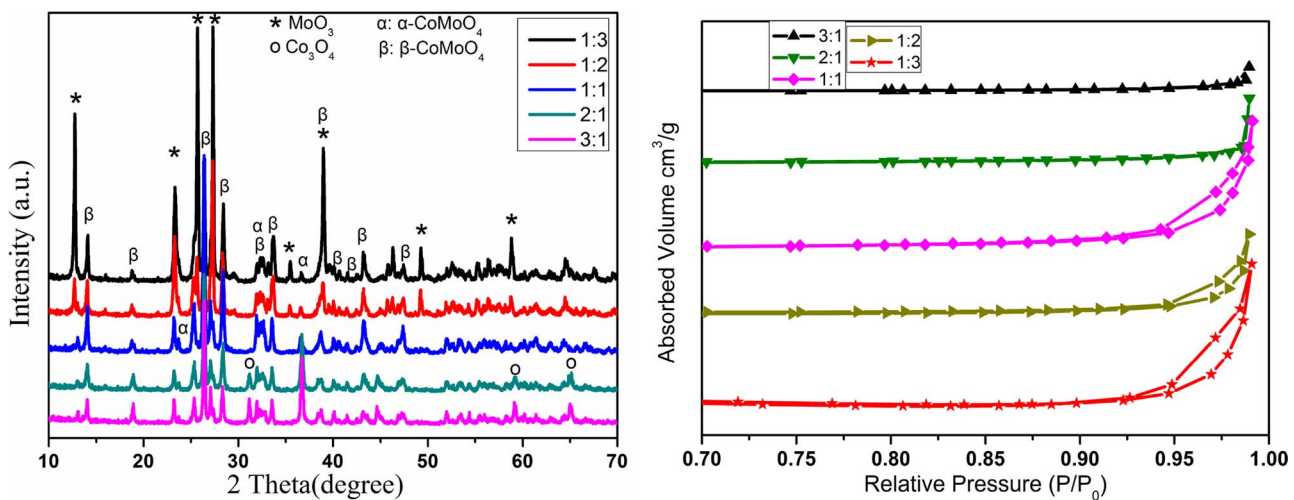


Fig. 1. XRD patterns (A) and N₂ adsorption-desorption isotherms (B) of samples with different Co/Mo ratios (1:3, 1:2, 1:1, 1:2 and 1:3).

with the desired amounts of the starting cobalt nitrate and ammonium heptamolybdate, denoted as Co/Mo (x:y). For comparison, single metal oxides such as Co₃O₄ and MoO₃ were also prepared, respectively.

2.2. Characterization techniques

The crystal structures of catalysts were analyzed on a Bruker D8 ADVANCE diffractometer operated at 40 kV and 40 mA with CuK α radiation source of wavelength 1.542 Å. The morphologies of catalysts were investigated by scanning obtained on a Hitachi S-4800 microscope, while the transmission electron microscopy (TEM) micrographs were collected in a JEOL-JEM-2100 microscope operating at 200 kV. The surface area and pore size distribution of catalysts were obtained from N₂ adsorption/desorption isotherms measured by a Tristar 3000 sorptometer. Prior to the analysis, the catalysts were degassed at 160 °C under vacuum for 2 h. Raman spectroscopic measurements were carried out with a Renishaw in Via Raman Microscope system using a 514.5 nm laser as the excitation source. A laser output of 30 mW was used, and the maximum incident power at the sample was approximately 6 mW in each measurement. Fourier Transform Infrared Spectroscopy (FT-IR) of KBr pellets were performed with an AVATAR 370 Thermo Nicolet spectrophotometer with a resolution of 2 cm⁻¹. Diffuse reflectance UV-vis (DRUV) spectra were recorded in the wavelength range of 200–800 nm using a Varian-Cary 5000 spectrometer with a diffuse reflectance attachment to assess the nature of Co and Mo species. The surface electronic states of catalysts were investigated by X-ray photoelectron spectroscopy (XPS, Axis Ultra, Kratos Analytical Ltd.) with a monochromatic X-ray source of Al K α radiation under ultra-high vacuum ($3\text{--}2 \times 10^{-6}$ Pa). The binding energies (± 0.2 eV) were internally calibrated by the reference deposit C1 s binding energy (284.8 eV). The obtained spectra were fitted by mixed Gaussian-Lorentzian functions.

2.3. DFT calculations

The energy and geometrical structures of the smallest model CoMoO₄ (a) was optimized using a LANL2DZ basis set for Co and Mo and a 6-31G(d, p) basis set for O atom. In addition, three different adsorbate-CoMoO₄ complex structures with similar computational methods have been considered [21–23]: one formed by peroxide and the Mo = O site of CoMoO₄ model (b), and the other two formed by molecular oxygen approaching the CoMoO₄ model in two different active sites (Co site for (c) and Mo site for (d)). All the calculations were performed with the Gaussian 09 program, and no imaginary frequencies in the obtaining vibrational information in the calculation

were observed in any of the situations presented in this work. Natural bond orbital (NBO) analyses were further performed by the same basis set on the optimized structure to gain insight into the electronic distribution and bonding patterns of these models.

2.4. Catalytic aerobic epoxidation of alkenes to epoxides

Liquid phase oxidations of cyclohexene with labile allylic hydrogen atoms using ethylbenzene as a solvent were carried out in a Teflon-lined 100 cm³ stainless-steel autoclave reactor, containing a magnetic stirrer. Typically, cyclohexene (1.5 g, purified by passing it over activated alumina to eliminate the hydroperoxide), ethylbenzene as solvents (8 g) and catalysts (0.2 g) were placed into the reactor in one lot; the autoclave was hermetically sealed and heated to 130 °C. Oxygen was then charged into the reactor to the desired pressure (0.6 MPa) and the reaction was started by adjusting the stirrer speed to 400 rpm. After the reactions, the mixture was cooled down and the catalyst was separated by filtration. The liquid organic products including the solvent oxidation products were identified by GC-MS (comparison with commercially available standards) and quantified with a gas chromatograph (Agilent 6890N), equipped with a polysiloxane capillary column (DB-17, 30 m × 0.32 mm × 0.50 μm) and a FID detector, using chlorobenzene as the internal standard. Both the injector and detector temperature were 280 °C, and the column temperature was 160 °C. The yields of 2-cyclohexen-1-ol and 1-phenylethanol were calculated as the difference between the value obtained by GC and the concentration of hydroperoxide determined iodometrically (reduction in 3-hydroperoxyoctahydro-1-ene and EBHP with PPh₃ gives an additional amount of 2-cyclohexen-1-ol and 1-phenylethanol, respectively). The gas composition was analyzed by gas chromatography with TCD detector and mass balance was verified.

3. Results

3.1. Characterization of the catalysts

3.1.1. Crystal structure and textural property

The XRD patterns of hollow CoMo bimetallic catalysts with various Co/Mo ratios are shown in Fig. 1A. For all the prepared catalysts, the diffraction peaks at $2\theta = 12.6^\circ$, 23.3° , 25.7° , 27.3° , 35.5° , 39.0° , 49.2° and 58.8° are observed, which can be ascribed to the crystalline phase of MoO₃ [24]. The typical diffraction peaks of MoO₃ gradually decrease and shift to lower degrees with increasing Co/Mo ratios, which indicates that the Co species enters the lattice of MoO₃ and results in the expansion of lattice due to the larger ionic radius of Co²⁺. Meanwhile,

this also suggests that MoO_3 is gradually dispersed on the catalyst and the particle size of MoO_3 crystallites is decreased. Additionally, the diffraction peaks at 13.7° (001), 18.8° (201), 26.3° (002), 28.4° (311), 32.1° (131), 32.7° (022), 33.7° (222), 36.7° (400), 38.7° (040), 40.1° (003), 41.5° (222), 43.4° (223), and 47.4° (421), assignable to the β - CoMoO_4 phase (JCPDS card 21–868), are observed for all the samples except the diffraction peaks of MoO_3 . Actually, the β - CoMoO_4 phase can be achieved during calcination at 500°C , since that β -phase is the more stable form of CoMoO_4 . As a result, the coordination around the molybdenum center is mainly distorted tetrahedral in CoMo bimetallic catalysts, similar reports found in β - CoMoO_4 phase [25]. Additionally, an interesting phenomenon is that the full width at half maximum (FWHM) of CoMoO_4 peak at 26.3° (002) increases with increasing amounts of cobalt, which indicates that a dominant β - CoMoO_4 phase in the hollow CoMo bimetallic catalysts can be obtained in the XRD spectra of the sample with a Co/Mo = 1:1. If the Co/Mo ratio is further increased to 2:1, the obvious diffraction peaks at $2\theta = 31.2^\circ$ (220), 59.1° (511), and 65.1° (400) are also observed, which can be ascribed to the Co_3O_4 crystalline [26]. This can be explained by the fact that only appropriate Co species can be accommodated in the structure of MoO_3 to form CoMoO_4 phase, and the excessive Co_3O_4 crystalline may be formed on the surface of CoMoO_4 . Mainwhile, the conversion of CoMoO_4 from β -phase to α -phase may occur in the excess of cobalt species. These diffraction lines provide clear evidence of the alteration of the original electronic and geometric structure of CoMoO_4 by the introduction of Co species.

N_2 adsorption/desorption isotherms for the synthesized hollow CoMo bimetallic samples are shown in Fig. 1B, and the specific surface area, total pore volume, external surface area and pore size are listed in Table 1. For each of the synthesized samples, the presence of the intraparticle voids is evident from abrupt closure at $p/p_0 = 0.93$ on the desorption branch. Interestingly, the increase of Co/Mo ratio leads to a drastic decrease of N_2 quantity adsorbed, which indicates that the Co content of samples strongly affects the size range of the intraparticle voids. In addition, the synthesized hollow CoMo bimetallic catalysts essentially differ in their textural properties (Table 1). With the Co/Mo ratio from 1:3 up to 1:1, the specific surface area and pore volume of the samples correspondingly increases from 4.83 to $21.84 \text{ m}^2/\text{g}$, and from 0.002 to $0.056 \text{ cm}^3/\text{g}$; external surface area increases from 4.53 to $17.2 \text{ m}^2/\text{g}$. However, the pore volume and pore size are apparently decreased when more $\text{Co}(\text{NO}_3)_2 \cdot 6\text{H}_2\text{O}$ was used in the precursor synthesis, which may be caused by the excess of cobalt species in the form of Co_3O_4 crystalline (as observed by XRD analysis) due to the possible blocking or covering of the intraparticle voids in the samples. Thus, the well-defined hollow structure can facilitate diffusion and accessibility of guest molecules.

The TEM images of hollow CoMo (Co/Mo = 1:1 and Co/Mo = 2:1) bimetallic catalysts calcined at 500°C are presented in Fig. 2. The images of the Co/Mo = 1:1 sample display that cobalt molybdate consists of aggregates of crystalline particles in the 50–250 nm size range (Fig. 2). The obvious lighter contrast regions (2–20 nm in size as indicated in Figs. 2A₁ and 2B₁) confirms that the catalysts contain intraparticle voids, and the intraparticle voids are located exclusively in the inner part of the crystals and never communicate directly with the

surface (as observed by N_2 adsorption/desorption analysis). When compared with the Co/Mo = 1:1 sample, the Co/Mo = 2:1 materials retain their intraparticle-void structures as indicated by the 1–5 nm lighter contrast regions in Fig. 2B₁ and 2B₂, which implies that the introduction of excessive cobalt species to the hollow CoMo bimetallic materials can change the size range of the intraparticle voids. In addition, the Co/Mo = 2:1 materials consist of fairly uniform crystalline particles, which is seemed to shrink to a smaller size (50–100 nm). The data show that the Co content of samples strongly affects the morphology of average particle and average internal voids. Further, the HRTEM image of the magnified view of the Co/Mo = 1:1 sample is given in Fig. 2A₃. As can be seen, one sets of uniform fringe is found and the lattice fringe of 0.336 nm matches well with the (002) plane of cobalt molybdate phase [27]. Analysis of HRTEM micrographs of the Co/Mo = 2:1 sample shows that the increase of Co content in samples leads to a small fraction of crystalline or amorphous cobalt oxide layer forming on the surface of cobalt molybdate phase (Fig. 2B₃). Such little changes may be explained by weakening the interaction between active cobalt species and modified cobalt molybdate phase, and should have significant effect on catalytic activity of hollow CoMo bimetallic catalysts. Moreover, two other sets of different fringes are observed except for CoMoO_4 (220) fringes (0.336 nm) [27]: the lattice fringe of 0.244 nm can be indexed to the (311) crystal plane of Co_3O_4 , while the fringe of 0.213 nm corresponds to the (200) plane of CoO. Energy dispersive X-ray spectroscopy (EDS) of the Co/Mo = 1:1 materials displays the presence of cobalt, molybdenum, oxygen, and copper elements, as shown in Fig. 2C. The presence of copper element is due to the conductive copper tape used in the EDS measurement. These three elements are distributed homogeneously in the selected portion of the sample at submicrometer scale.

3.1.2. Surface composition and structure

As the catalysts studied contain d^0 transition metal oxide species (MoO_3) and d^5 (CoO), the hollow CoMo bimetallic catalysts (Co/Mo = 1:3, 1:2, 1:1, 2:1 and 3:1) have been characterised by Raman spectroscopy (Fig. 3A) and compared to MoO_3 , Co_3O_4 and their physical mixtures. For the bulk MoO_3 , the characteristic sharp bands of crystalline MoO_3 at 997, 821, 669, 379, 338 and 291 cm^{-1} appear, which be attributed to the terminal Mo = O symmetric stretching, symmetric or asymmetric Mo–O–Mo stretching vibrations in the $\text{Mo}_{8}\text{O}_{26}^{4-}$, bending of terminal Mo = O and the bridging Mo–O–Mo deformation in the $\text{Mo}_7\text{O}_{24}^{6-}$ octahedral species, respectively [28,29]. For the bare Co_3O_4 , five main signals can be also observed: the strong band at 678 cm^{-1} originates from the Raman active mode of octahedral sites (CoO_6 , $\text{Co}^{3+} - \text{O}^{2-}$) due to the A_{1g} species in the O_7^{h} spectroscopic symmetry; the bands with weak intensity at 477, 521 and 613 cm^{-1} are associated with E_g and F_{2g}^{2} symmetry; the other medium band located at 190 cm^{-1} is assigned to the F_{2g}^{1} Raman active mode of tetrahedral sites (CoO_4 , $\text{Co}^{2+} - \text{O}^{2-}$) [30,31]. Obviously, the hollow CoMo bimetallic catalysts with the low Co/Mo ratios (1:3 and 1:2) present the Raman band characteristic of pure crystalline MoO_3 (Fig. 3A). Some remarkable modifications of these signals with regard to broadness and position, however, are also detected. For instance, the characteristic bands at 997, 821, 669, 379, 338 and 291 cm^{-1} become broader and shift to higher frequencies (higher energies), which may originate from the distortions of the relaxation energy of the phonon promoted by alteration of the metal oxide structure [32]. Thus, these alterations indicate the modification of the vibrational structure of the crystalline MoO_3 . In addition, these characteristic bands are distinguished for Co/Mo > 0.5, which is due to that there are more Co atoms available to react with Mo to form Co–O–Mo bridging bonds. This also strongly confirms this assertion. On the other hand, the peaks of hollow CoMo bimetallic catalysts (Co/Mo = 1:1, 2:1 and 3:1) with comparsion of pure Co_3O_4 , especially for the vibration peaks of $\text{Co}^{2+} - \text{O}^{2-}$ and $\text{Co}^{3+} - \text{O}^{2-}$, become broader and shift to lower frequencies. In this sense, Ganduglia-Pirovano et al. [33] have proposed that the formation

Table 1
Textural property of the different samples (Co/Mo ratios = 1:3, 1:2, 1:1, 1:2, 1:3).

Catalyst	S_{BET} (m^2/g)	S^{ext} (m^2/g)	Pore size (nm)	Pore volume (cm^3/g)
Co:Mo = 1:3	4.83	4.53	11.62	0.002
Co:Mo = 1:2	9.11	8.07	11.36	0.023
Co:Mo = 1:1	21.84	17.21	13.08	0.056
Co:Mo = 2:1	17.83	12.60	5.34	0.017
Co:Mo = 3:1	15.23	9.83	4.35	0.011
MoO_3	0.84	0.15	12.94	0.003
Co_3O_4	5.44	3.75	3.64	0.050

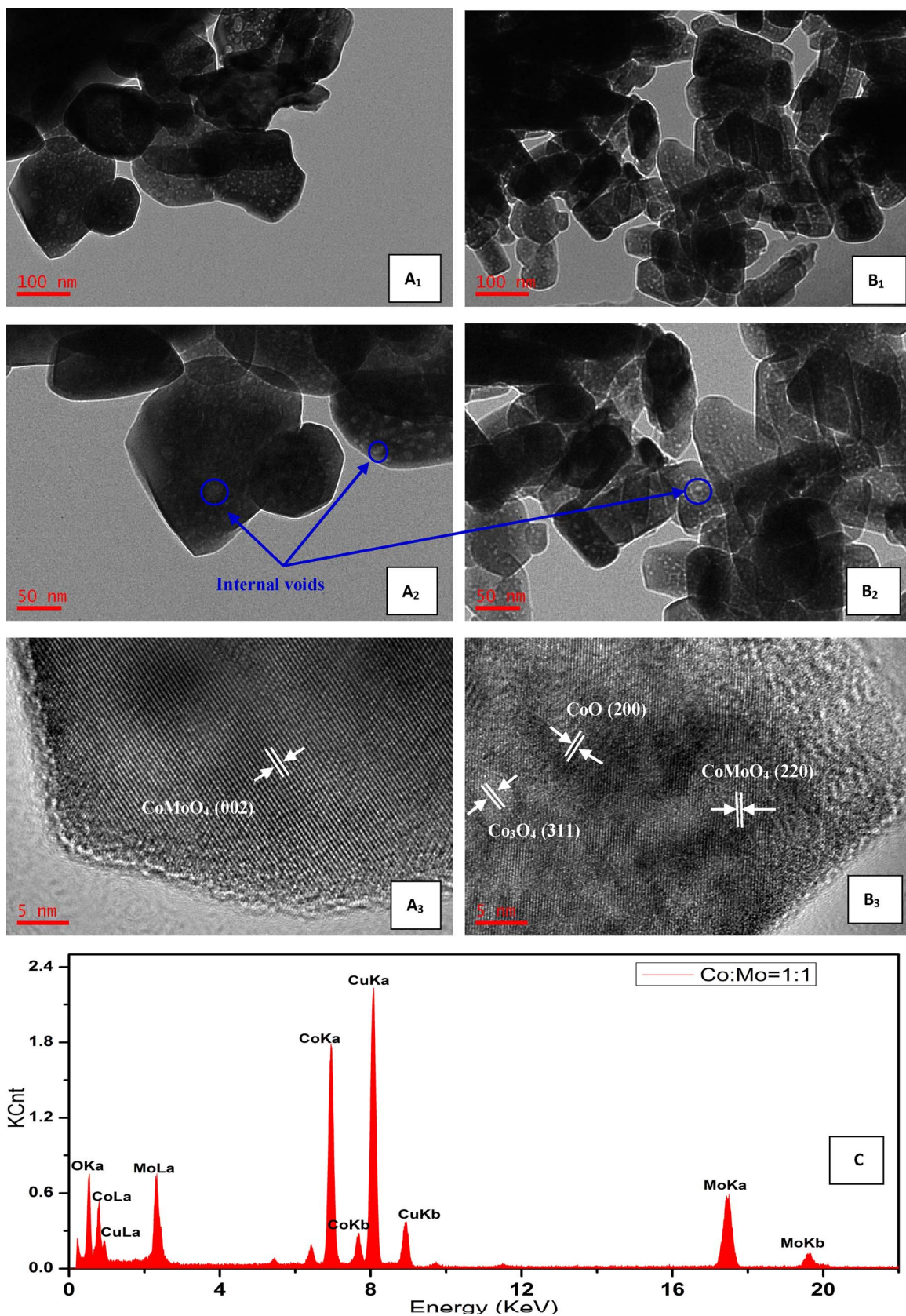


Fig. 2. TEM images of Co/Mo = 1:1 sample (A₁, A₂ and A₃) and Co/Mo = 2:1 sample (B₁, B₂ and B₃); X-ray spectroscopy (EDS) of Co/Mo = 1:1 sample (C).

of oxygen vacancies represents an alteration of the symmetry and the electronic distribution of the network (which is evenly shared by the different metallic atoms of the oxide). Therefore, we can conclude that

the introducing of MoO₃ modifies the electronic distribution of the Co₃O₄, which is thought to be favorable for the formation of oxygen vacancies and weakening the Co–O bond strength. Of interest is that

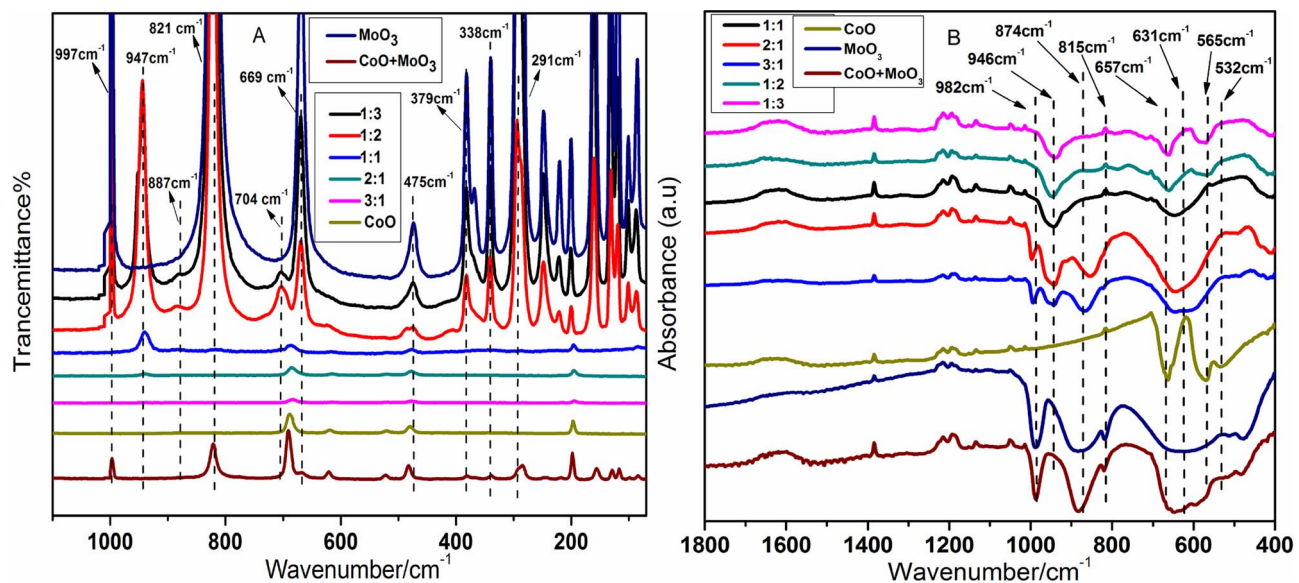


Fig. 3. Visible Raman spectra (A) and FT-IR spectra (B) of samples with different Co/Mo ratios (1:3, 1:2, 1:1, 1:2, 1:3, Co₃O₄, MoO₃ and the physical mixture of MoO₃ and Co₃O₄).

three new characteristic bands at 997, 887 and 704 cm⁻¹, not observed for pure MoO₃ or Co₃O₄, are usually assigned to the stretching vibration of Mo—O in (Mo—O)_xMo—O—Co unit or that of Mo—O⁸⁻...Co⁸⁺, being indicative of the insertion of the part Co atoms into the crystalline MoO₃ framework to form monophasic CoMoO₄ [34]. By comparison with the spectral profile of hollow CoMo bimetallic catalyst (Co/Mo = 2:1), a spectral feature of Co₃O₄-MoO₃ physical mixture (Co/Mo = 2:1, prepared by a simple ball milling treatment procedure) with new characteristic bands at 997, 887 and 704 cm⁻¹, is not detected. This is another indication that the Co atoms is partly incorporated into the framework of crystalline MoO₃ to form monophasic CoMoO₄. Thus, a distorted tetrahedral MoO₄ unit with two Mo=O double bonds and two Mo—O single bonds appears to develop on the catalyst surface [35].

To get somewhat more insight in the structure of cobalt molybdate, Fig. 3B illustrates the FT-IR spectra for two monometallic and hollow CoMo bimetallic catalysts. On the monometallic MoO₃ catalyst, a sharp absorption band around 980 cm⁻¹ is characteristic of terminal molybdenum oxygen double-bond (Mo=O) stretching, indicating that the molybdenum atoms are electronically less saturated in comparison with the molybdenum atoms present in the Mo—O—Mo linkages [36]. Two somewhat broader peaks at 874 and 815 cm⁻¹ and a very broad peak at 631 cm⁻¹ correspond to the vibrational bands of Mo—O single bonds and Mo—O—Mo linkages in a tetrahedral [(MoO₄)²⁻, T_d], as well as more common octahedral [(MoO₆)⁶⁻, O_h], symmetry [36]. With regard to the hollow CoMo bimetallic catalysts, their FT-IR spectra in all cases show the Mo = O and Mo—O stretching bands characteristic of pure MoO₃. However, a considerable decrease in the intensity of these bands of the pure MoO₃ is observed, while one broad band appears towards higher frequencies and another band shifts to lower frequencies, which may be assigned to the presence of Mo—O and Mo=O groups side-on bound to the cobalt (Mo = O⁸⁻...Co⁸⁺ and Mo—O—Co bonds) to form CoMoO₄ phase. This agrees with the fact that the disappearance of the terminal Mo = O bond at 980 cm⁻¹ corresponds with the growth in intensity of the band at 946 cm⁻¹ with the Co/Mo > 1:1. A similar effect is observed by Scarano et al. [37], where the presence of small amounts of heteroatoms is enough to induce modifications in the framework stretching region. On the other hand, the typical IR absorption bands of the monometallic Co₃O₄ catalyst, located at 657, 565 and 532 cm⁻¹, corresponding to the Co—O—Co stretching vibration [38], are not observed. However, the Co—O—Co stretching vibration is red-shifted to the overlapping of vibrational bands of Mo—O single bonds

and Mo—O—Mo linkages and the band shape becomes broader, which is ascribed to strong interactions with MoO₃ species. In addition, the strong band at 943 cm⁻¹, which appears for hollow CoMo bimetallic catalyst, is absent in the FT-IR spectra of two monometallic catalysts. This new band at 943 cm⁻¹ corresponding to Mo—O—Co stretching may be from the CoMoO₄ phase in bimetallic catalyst [39]. As Co/Mo ratio increases from 1:3 to 3:1, the relative peak intensity of Mo—O—Co bonds within CoMoO₄ phase increases, and then decreases; additionally the peak intensity of Co—O—Co bonds at 657 and 565 cm⁻¹ gradually becomes stronger which is due to that CoO₆ domains grow in size. The formation of these Mo—O—Co bonds within hollow CoMo bimetallic catalyst leads to larger domains and to a narrowing of the HOMO-LUMO gap, as shown in the following UV-vis DRS absorption. The current FT-IR findings are in excellent agreement with the Raman analysis on the preparation and tunability of hollow CoMo bimetallic catalysts and demonstrate that the hollow CoMo bimetallic oxide (Co/Mo = 2) phase is monophasic CoMoO₄ and free of excess octahedral CoO₆ species.

3.1.3. Electronic structure and chemical state

To obtain more information about the coordination environment of transition metal ions in the bimetallic catalysts, UV-vis diffuse reflectance spectroscopy is applied and the result is shown in Fig. 4. Since Mo⁶⁺ has a d⁰ electronic configuration, only absorption of MoO₃ corresponding to ligand-to-metal charge transfer (LMCT) O²⁻ (2p) → Mo⁶⁺ (3d) with comprising of a d-pπ* antibonding interaction between the Mo d_{xy} orbital and an O_{eq} p orbital, can be observed in the 200–360 nm region [40]. The exact position of the LMCT absorption bands is known to be sensitive to the local symmetry of the Mo⁶⁺ depending on their coordination and aggregation state [41]. For oxygen ligands, there are two characteristic LMCT bands in ranges 210–270 nm and 320–350 nm: the first one with a more energetic transition corresponds to the isolated molybdate species in tetrahedral coordination (T_d); the second one is assigned to polymeric octahedral Mo⁶⁺ species (O_h) [40]. Pronounced change in the peak position to a longer wavelength, as well as peak shape, is observed for the LMCT band of the bimetallic catalysts (Fig. 4). This can be attributed to the distortion of the symmetry of the [MoO₄] tetrahedra or [MoO₆] octahedra structure assigned to the formation of an interfacial Mo = O⁸⁻...Co⁸⁺ and Mo—O—Co bonds. In this sense, the red shift of LMCT band actually occurs. Thus, the large energetic stabilization of the lowest unoccupied molecular orbital (LUMO), coupled with a favorable overlap between

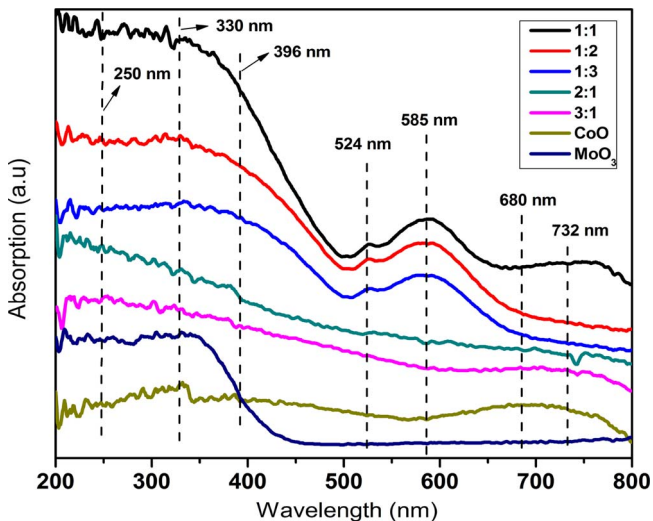


Fig. 4. UV-vis spectra (A) of samples with different Co/Mo ratios (1:3, 1:2, 1:1, 1:2, 1:3, Co_3O_4 and MoO_3).

the cobalt-bound highest occupied molecular orbital (HOMO) and the O_{eq} p orbital of the LUMO, facilitates substrate attack at this position [42]. At the same time, a reduction in the activation energy for the oxygen atom transfer reactions undoubtedly results from the nature of the heterodinuclear $\text{Mo} = \text{O}_{\text{eq}}$ d-p π^* interaction, which facilitates

cleavage of the $\text{Mo} = \text{O}_{\text{eq}}$ bond and promotes product release (when occupied by the O lone pair in the Co–O bond). Thus, the unique electronic structure imposed by the low symmetry of the Co–O bond may contribute substantially to the difference between the oxygen atom transfer reactions rate of the bimetallic catalysts compared to that of monometallic catalysts.

On the other hand, the UV-vis spectra of Co_3O_4 in Fig. 4 present two broad absorption bands centered at 396 and 680 nm, which corresponds to the LMCT $\text{O}^{2-} \rightarrow \text{Co}^{2+}$ with basic optical band gap energy and $\text{O}^{2-} \rightarrow \text{Co}^{3+}$ with Co^{3+} level located below the conduction-band, respectively [43]. However, a shift of absorption edge to lower energy with comparison of monometallic Co_3O_4 is observed for the bimetallic catalysts. Especially for the hollow CoMo bimetallic catalysts with the lower Co/Mo ratios (1:3, 1:2 and 1:1), the change in the red-shift of absorption edge is much more clear, which is due to that the introducing of MoO_3 decreases the band gap energy and promotes the electron-transition from HOMO to LUMO. Based on the results of Iglesia et al., the electron transfer normally occurs among the transit of exciting electrons from the HOMO to LUMO, and the cleavage of a weaker metal–oxygen bond results in a lower energy for the catalytic redox cycle [44]. Interesting, the visible spectra of the bimetallic catalysts present new bands in the 500–600 nm region, not observed for monometallic MoO_3 or Co_3O_4 catalyst, are usually ascribed to d-d transitions [${}^4\text{T}_{2g} \rightarrow {}^4\text{A}_{2g}$ and ${}^4\text{T}_{2g} \rightarrow {}^4\text{T}_{1g}(\text{P})$] of high spin Co^{2+} ions in an octahedral coordination environment, as similar found in monophasic CoMoO_4 [45]. This is indicative of the interaction of part Co^{2+} ions with the Mo^{6+} species. The intensity of these peaks increases with

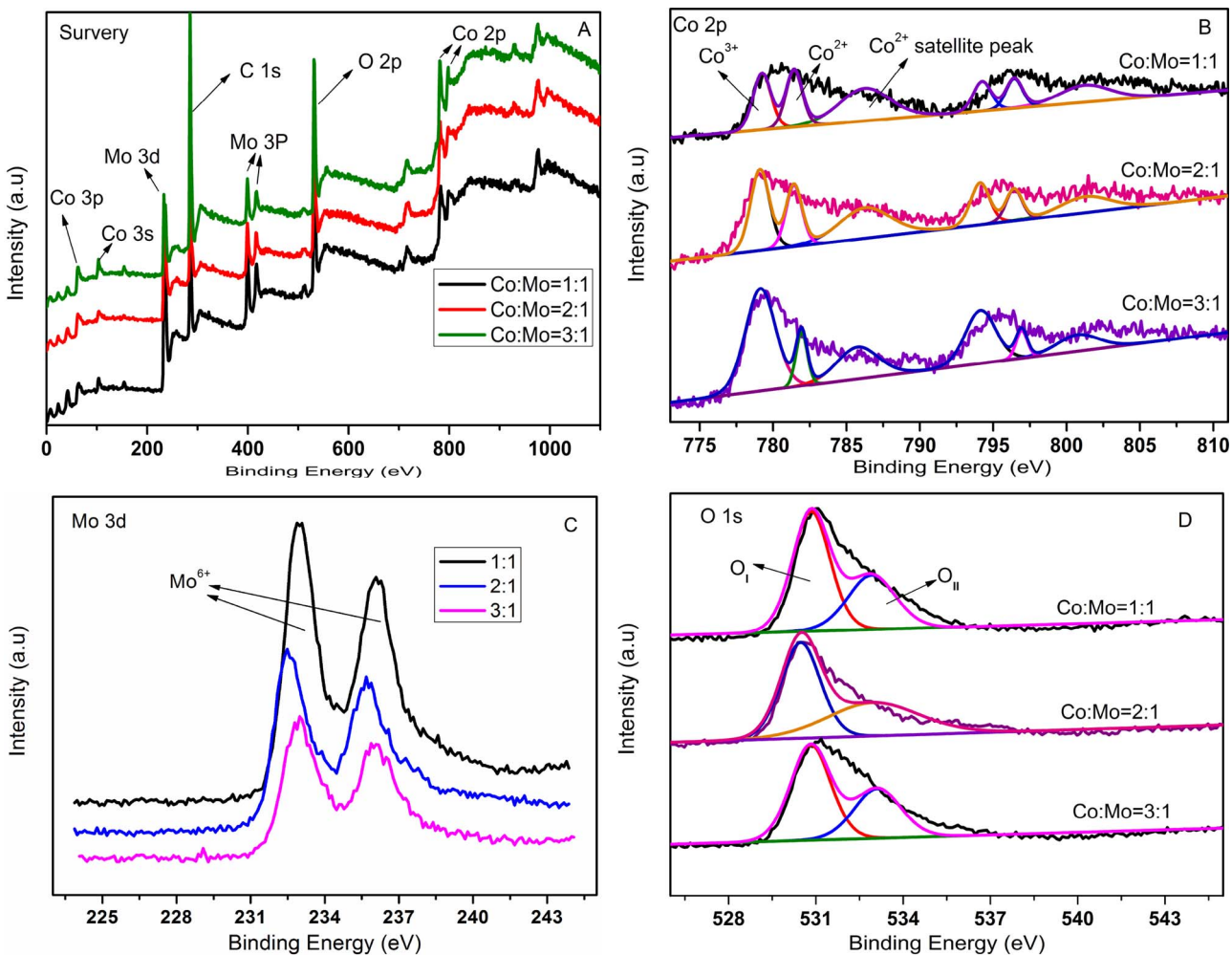


Fig. 5. Survey spectrum of samples (A) and XPS spectra of Co 2p (B), Mo 3d (C) and O 1 s (D) of samples (1:1, 1:2 and 1:3).

decreasing Co/Mo ratios (1:1, 1:2 and 1:3), indicating that the amount of CoMoO₄-like Co species increases. Additionally, the spectrum for the Co/Mo ratios (1:2) is very similar to that of the Co/Mo ratios (1:3) catalyst. By contrast, the shape of the spectrum of the high Co/Mo ratios (3:1 and 2:1) catalyst is completely different from that of Co/Mo ratios (1:3) catalyst and exhibits the appearance of a red-shift band at 732 nm as found in the monometallic Co₃O₄ catalyst (680 nm). Therefore, we can concluded that the bimetallic catalysts with the low Co/Mo ratio show most of the Co species bonding with Mo species (the formation of Mo—O—Co bonds). As the Co/Mo ratio increase, however, free Co species begin to appear and weakly interact with Mo species (Mo = O^{δ-}...Co^{δ+}). As a result, the spectrum of the hollow CoMo bimetallic oxide (Co/Mo = 2) may be rationalized as a sum of contributions from two types of species: one bonding with Mo to form Mo—O—Co bonds (band at 580 nm) and a second one in which the Co species weakly interact with Mo (band at 732 nm).

XPS spectra are measured to investigate the surface properties and chemical state of the hollow CoMo bimetallic catalysts. A good separation of the peaks assigned to the Mo 3d_{5/2} and Mo 3d_{3/2} photoelectrons [46] is reported in the XPS survey spectra of the Co 2p and Mo 3d photoelectrons, as plotted in Fig. 5A. The binding energies (BEs) of the strong intense photoelectron Mo 3d compared with that of Co 2p is also observed, which may be attributed to the good evidence that the 2p signal of the transition-metals in the fourth period is inherently weaker than the 3d signal of the transition-metals in the fifth period. The Co 2p spectra are characterised by the two spin-orbit components (2p_{3/2} and 2p_{1/2}) and the presence of two intense shake-up satellites typical of high spin Co²⁺ species [47] (in Fig. 5B). The Co 2p_{3/2} signal of the bimetallic catalysts can be further resolved into two parts according to the references [43], one at low energy corresponding to Co²⁺ in CoO or Co²⁺ in CoMoO₄ and the other at higher value corresponding to a Co³⁺ in Co₃O₄. Based on previous studies [27,45], Co²⁺ in CoMoO₄ (783.3–783.5 eV) has a relatively larger BE deviation as compared with that of Co²⁺ in CoO (780.9–781.0 eV), which may be due to the presence of the polarization effect or the nonstoichiometry with Co²⁺ species being incorporated into highly oxidized crystalline Mo₃O₈ matrix [45]. However, the BE values are too close to be clearly identified and a more convincing evidence for this conversion can be obtained by evaluation of the shake-up satellite peaks with 6.0–6.5 eV higher than the primary spin-orbit BEs (I_p/I_s). The intensities of these shake-up peaks satellites associated with the Co 2p_{3/2} of CoO from Co₃O₄ or CoMoO₄ has often been used for the identification of the special Co oxide species [48]. Usually, the Co₃O₄ compounds being a normal spinel contain two distinct Co²⁺ ions in four-fold coordination to oxygen and Co³⁺ in six-fold coordination to oxygen in the ratio of 1:2; this satellite peak of Co²⁺ is very small in the spectrum of Co₃O₄ but very strong in the spectrum of CoMoO₄ [48]. A clear trend is observed in Fig. 5B and Table 2 for the relative intensities and I_p/I_s. The intensity ratio for the low Co/Mo ratio (1:1) catalyst is high and close to that of stoichiometric CoMoO₄ (0.79), but gradually decreases toward the value of Co₃O₄ (0.3) when the Co/Mo ratios increases. This trend suggests that the concentration of Co₃O₄ increases on the surface of the catalysts at expenses of the concentration of CoMoO₄. On the other hand, in order to determine the possible Co oxide species and exact geometry of the cobalt ions with respect to neighboring atoms present in catalysts, the spin-orbit splitting (ΔE_1) and the energy difference between the

principal photopeak and the satellite peak (ΔE_2) are taken into account [48]. According to previous studies of Oku et al. [49], i) ΔE_1 values are affected by the oxidation state: ca. 15 eV for diamagnetic cobaltous compounds (Co³⁺) and ca. 16 eV for paramagnetic cobaltous compounds (Co²⁺); ii) ΔE_2 values are affected by the coordination of Co²⁺ to neighboring oxygen atoms: ca. 5 eV for tetrahedral coordination of Co²⁺ and ca. 6 eV for octahedrally coordinated Co²⁺. Thus, the values (ΔE_1 : 16.41 eV and ΔE_2 : 5.87 eV) reported in Table 2 for the Co 2p XPS spectrum of the catalyst with Co/Mo ratios = 2:1 suggest that a majority of the Co²⁺ species in octahedrally coordinated environment is present in the catalyst surface. In addition, the BEs of Co²⁺ and Co³⁺ on the surface of bimetallic oxide are shifted to the lower BEs compared with that of pure Co₃O₄ [43], which indicates the modification on electronic structure of the surface Co₃O₄ present in the bimetallic catalysts.

The Mo 3d spectra show the two spin-orbit components (3d_{5/2} and 3d_{3/2} with an energy separation of 3.1 eV), and the BEs are typical of Mo⁶⁺ [24]. The broadness of the peaks shown in Fig. 5C is an indication of several Mo⁶⁺ oxo-species [50]. Obviously, a slight broadening of the FWHM with the increment in the Co/Mo ratios are observed in Table 2. The broadening of the peaks can be attributed to the cobalt-induced transformation of the monomeric Mo species (MoO₄²⁻) into polymolybdate species (Mo₇O₂₄⁶⁻) as suggested by other authors [51], which is in good agree with the observed in XRD results. Concerning the distribution of Mo and Co at the catalyst surface, as observed from the XPS derived atomic percentages (in Table 2), the catalyst with Co/Mo ratio (2:1) is almost the same surface atomic concentrations of Co and Mo with respect to the analytical contents, indicating that the excess of cobalt species are distributed on the inner surface of the intraparticle voids. The O 1 s spectra (Fig. 5D) are fitted with two peaks at ca. 532.3 (O_I, main band) and 530.7 eV (O_{II}, shoulder band). The 532.3 eV peak with a higher BE is characteristic of the lattice oxygen bound to metal cations in metal oxide [27], whereas the one at 530.7 eV mainly corresponds to surface-adsorbed oxygen species on oxygen vacancies (attributed to a defect oxide) and surface hydroxyls associated with metal sites [26]. Therefore, the intensity ratio O_{II}/O_I is of great value to qualitatively estimate the relative abundance of surface oxygen vacancies. It is seen from Fig. 5D and Table 2 that the O_{II}/O_I ratio presents an increasing trend with the Co/Mo ratio from 1:1 to 2:1, and then decreases at the Co/Mo ratios of 3:1. As a result, a higher concentration of surface oxygen vacancies on the catalyst with Co/Mo ratio = 2:1 is formed, which may be attributed to the fact that surface oxygen vacancies can be developed by the stabilization of Co²⁺ species with the same number of Mo⁶⁺ sites (from the surface atomic concentration ratios) to form the larger amount of Co²⁺—O_V—Co²⁺ defect structures.

3.2. Catalytic activities

Direct aerobic epoxidation of alkenes catalyzed by the various hollow bimetallic CoMo oxides is investigated on cyclohexene containing labile allylic hydrogen atoms, known to be highly sensitive to auto-oxidation with mainly formation of radical allylic oxidation products; and the activity results compared with the corresponding monometallic oxides are listed in Table 3. As expected, the blank experiment without any catalyst shows that a 54% cyclohexene conversion with only small amounts of epoxidation products and allylic

Table 2
Some XPS features of samples with different Co/Mo ratios.

Catalyst	Co 2p _{3/2}		Co 2p relationships			O 1s		Mo 3d _{5/2}		Co/Mo ratios
	BE	FWHM	ΔE_1	ΔE_2	I _p /I _s	BE	FWHM	BE	FWHM	
1:1	781.98	3.19	16.19	4.81	0.63	531.09	2.54	232.97	1.51	0.82
2:1	781.11	4.18	16.41	5.87	0.56	530.65	2.44	232.53	1.61	1.09
3:1	781.38	3.72	15.80	6.01	0.46	531.25	3.04	232.94	1.85	1.69

Table 3Aerobic epoxidation of cyclohexene using ethylbenzene as a solvent catalyzed by hollow CoMo bimetallic catalysts^a.

Entry	Catalyst	Alkene conv. (%) ^b	Alkene epoxidation selectivity (%) ^c			EB conv. (%) ^b	EB peroxidation selectivity (%) ^c				
			Epoxide	Allylic oxidation			PA	AP	EBHP	Others ^d	
				Aol	Aone						
1	—	54.2	20.8	10.7	23.7	44.8	2.8	48.7	39.3	7.4	4.6
2	MoO ₃	7.1	73.1	12.8	7.1	7.0	1.3	78.9	17.7	0.9	2.5
3	Co ₃ O ₄	42.8	16.1	5.5	44.4	34.0	8.5	41.6	47.6	3.5	7.3
4 ^e	MoO ₃	8.3	48.0	19.8	31.1	1.1	—	—	—	—	—
5 ^f	MoO ₃	—	—	—	—	1.1	66.4	30.7	1.1	1.8	—
6 ^e	Co ₃ O ₄	14.7	22.1	9.5	64.2	4.2	—	—	—	—	—
7 ^f	Co ₃ O ₄	—	—	—	—	4.0	37.8	52.4	5.7	4.1	—
8 ^g	Co _{0.5} MoO ₃	24.4	30.2	8.8	33.2	27.8	3.8	55.5	36.5	2.6	5.4
9	Co/Mo = 3:1	36.7	42.8	9.6	9.8	37.8	4.6	59.6	32.0	2.1	6.3
10	Co/Mo = 2:1	33.9	59.1	9.1	12.2	20.6	4.3	72.1	21.6	1.2	5.1
11	Co/Mo = 1:1	11.6	62.6	19.3	10.5	5.8	1.8	78.0	17.5	0.7	3.8
12	Co/Mo = 1:2	11.0	63.9	18.0	10.9	5.3	1.9	78.9	16.2	0.8	4.1
13	Co/Mo = 1:3	11.3	65.7	15.4	11.3	5.6	2.0	78.0	17.8	0.6	3.6
14 ^h	Co/Mo = 1:2	22.8	51.3	—	41.2	7.5	3.1	73.4	21.4	0.9	4.3
15 ⁱ	Co/Mo = 1:2	9.5	98.1	—	—	1.9	1.2	83.9	13.5	0.4	2.2
16 ^j	Co/Mo = 1:2	61.8	18.6	2.6	5.9	72.9	—	—	—	—	—
17 ^k	Co/Mo = 1:2	15.2	12.6	1.7	53.1	32.6	—	—	—	—	—
18 ^l	Co/Mo = 1:2	—	—	—	—	—	—	—	—	—	—
19 ^m	Co/Mo = 1:2	3.7	32.2	17.9	0.8	49.1	—	—	—	—	—

^aAll reactions were done with 0.20 g of catalyst, 1.5 g cyclohexene, 8.0 g of ethylbenzene, 0.6 MPa O₂, 130 °C, time (1 h).^bConversion (%) based on substrate = {1 – [(concentration of substrate left after reaction) × (initial concentration of substrate) – 1]} × 100, EB: ethylbenzene.^cProduct selectivity = content of this product/(adding cyclohexene or ethylbenzene amount (mmol)-the amount of cyclohexene or ethylbenzene recovered (mmol)) × 100%, PA: 1-phenylethanol, AP: acetophenone, EBHP: ethylbenzene hydroperoxide.^dOthers, alkene epoxidation: cyclohexane-1,2-diol and non-detected products by GC; EB peroxidation: benzaldehyde, benzoic acid and small amounts of unidentified products.^eUsing cyclohexene (10.0 g) instead of a mixture of cyclohexene and ethylbenzene, 80 °C.^fUsing ethylbenzene (10.0 g) instead of a mixture of cyclohexene and ethylbenzene.^gA physical mixture of MoO₃ and Co₃O₄ (Co/Mo = 2:1).^hUsing cyclopentene or 1-octene (1.5 g) instead of cyclohexene.^{j,k,l}Using cumene, toluene or DMSO (8.0 g) instead of ethylbenzene.^mAddition of hydroquinone as a free radical scavenger (5 mol% cyclohexene).

oxidation products (such as 2-cyclohexen-1-ol and 2-cyclohexen-1-one) are obtained, as a result of radical polymerization and the abstraction of allylic H atom by ·OH radicals produced in the thermal auto-oxidation process (entry 1). For Co₃O₄, cyclohexene conversion decreases up to 42.8% and allylic oxidation product 2-cyclohexen-1-one selectivity increases close to 45%, but epoxidation product selectivity is only 16.1% along with 5.5% 2-cyclohexen-1-ol (entry 3). As can be argued from the product distribution, the allylic oxidation mechanism, proceeding via α-H-abstraction and generation of an allylic radical, seems to be the main operating oxidation or deep-oxidation path. Meanwhile, the same experiment but with MoO₃ instead of Co₃O₄ gives good epoxide selectivity (> 70%), but cyclohexene conversion was remarkably lower over this sample (entry 2). In striking contrast, about 34% of the cyclohexene is converted with hollow bimetallic CoMo oxides under the same conditions, and the selectivity to 1,2-epoxycyclohexane is 59% (entry 10). These results indicate that the cooperativity between Co sites and Mo sites can inhibit the allylic oxidation route to form allylic oxidation products and enhances the catalytic performance for epoxidation of cyclohexene to form 1, 2-epoxycyclohexane. Moreover, a physical mixture of MoO₃ and Co₃O₄ (referred to as the hollow CoMo oxide with Co/Mo ratios = 2:1) is used as a catalyst. Low catalytic activity and 1, 2-epoxycyclohexane selectivity, however, are obtained under similar conditions (entry 8). This appears to reflect the higher reactivity of Mo–O–Co or Mo–O^{δ−}...Co^{δ+} unit (from characterization results) for selective epoxidation of cyclohexene to form epoxide compared with that of monometallic oxide with unmodified electronic

structure.

To study synergistic effects in affecting the reaction route, we further study the effect of Co content on the catalytic behavior, and Table 3 demonstrates the effect of Co/Mo ratio on catalytic performance of the hollow CoMo bimetallic catalysts. As the Co/Mo ratio rise from 1:3 to 1:1, the cyclohexene conversion almost keeps constant, and the selectivity to epoxide slightly decreases from 65.7% to 62.6%, indicating that the Mo–O–Co or bridging sites is beneficial for obtaining a higher epoxide selectivity (entries 11, 12 and 13). When the Co/Mo ratio further increases, for instance, from 1:1 to 1:2, the cyclohexene conversion increases sharply with 59% epoxide selectivity, which may be attributed to the fact that surface oxygen vacancies for oxygen activation can be developed by the stabilization of Co²⁺ species with the Mo–O–Co bridging sites (entry 10). However, the epoxidation product selectivity decreases sharply from 59.1% to 42.8%, and cyclohexene conversion does not change significantly if the Co/Mo ratio further increases to 3:1 (entry 9). It may be due to that the increase of surface density of Co species covers the active sites such as Mo–O–Co bridging sites with restricting the epoxidation of cyclohexene. Obviously, the analytical data shown in Table 3 demonstrates that the selectivity to epoxide can be tuned using hollow CoMo bimetallic catalysts by controlling the Co/Mo ratio.

To gain insights into the roles of the Co species and Mo species in the different oxygen transfer processes, two sets of separate experiments have also been tested, the first one is investigated with the addition of pure cyclohexene instead of the corresponding mixture

(cyclohexene and ethylbenzene) over the pure Co_3O_4 or MoO_3 catalysts, respectively (entries 4 and 6). Interesting, the rate of product formation with the pure Co_3O_4 is almost two orders higher than that with the MoO_3 catalysts; moreover, our observation that the higher epoxide selectivity maintained with MoO_3 differs greatly from that of the Co_3O_4 catalyst. For Co_3O_4 , the ionic radius of Co^{2+} (0.65 \AA) is larger than that of Mo^{6+} (0.59 \AA), and thus bonding energy of $\text{Co} – \text{O}$ is lower than that of $\text{Mo} – \text{O}$. A plausible explanation for this promotional effect of Co_3O_4 on cyclohexene conversion has been given by Giamello and co-workers [52]: the Co sites with the low bonding energy on the oxide surfaces can easily adsorb and activate oxygen, allowing O_2 and cyclohexene to easily react together thus giving a high reaction rate. However, Co_3O_4 does not efficiently catalyze olefin epoxidation. While in the second experiment, the oxidation of pure ethylbenzene instead of the corresponding mixture (cyclohexene and ethylbenzene) over the pure Co_3O_4 or MoO_3 catalysts is also tested, respectively. In fact, it's found that the higher ethylbenzene conversion and EBHP concentration are obtained for ethylbenzene oxidation with Co_3O_4 , where only traces of the EBHP are served with MoO_3 (entries 5 and 7). These results suggest that Co species can activate effectively molecular oxygen mediate the first step of the overall oxidation cycle yielding an EBHP by peroxidation of solvents, as shown in Table 3. However, if the EBHP formed in reaction system is not consumed rapidly by oxygen transfer process to make the epoxide, they can give a large number of undesired allylic oxidation reactions or radical polymerization with low epoxide selectivity. On the other hand, 1-phenylethanol is detected as the main products when a higher selectivity to epoxide is obtained (Table 3), which further indicates that oxygen atom of epoxide from the selective decomposition of EBHP is efficiently transferred to the cyclohexene (main acetophenone is formed by non-selective decomposition in the case of EBHP). As a result, Co-modified Mo sites behave very uniquely for the epoxidation of cyclohexene, which are shown to be the excellent catalytic sites for the subsequent epoxidation step by the transfer of oxygen atom of the EBHP to cyclohexene. These unique behaviors imply that the current catalyst may represent a novel-type Mo-based oxygen transfer catalyst whose electronic structure of active site is modified by the transition metal species.

We have clarified that the peculiar result that moderate epoxide selectivity can be maintained over the hollow CoMo bimetallic catalysts stemming from the presence of the solvent as oxygen transfer agents. Therefore, an understanding of the primary solvent peroxidation process where can be easily form oxygen transfer agents, solvent is needed. Table 3 shows that neither cumene nor toluene is an efficient solvent, despite structural similarities containing the alkyl C–H bond (entries 16 and 17). Meanwhile, no oxidized products of toluene are detected by GC. Based on the optimization of the structures including alkylbenzene and the corresponding alkyl hydroperoxide by our DFT investigation, calculation results show the C–H bond length of the solvents with decreasing in order of cumene ($\text{H}-\text{C}(\text{CH}_3)_2-$, 1.09813 \AA) > ethylbenzene ($\text{H}-\text{CHCH}_3$, 1.09694 \AA) > toluene ($\text{H}-\text{CH}_2-$, 1.09574 \AA). Thus it is more easy for homolytic cleavage of the longer C–H bond of cumene to rapidly yield cumene hydroperoxide, as observed in a higher reaction rate. On the other hand, the O–O bond length of the alkyl hydroperoxides increases in the sequence cumene hydroperoxide ($\text{HO}-\text{O}-\text{C}(\text{CH}_3)_2-$, 1.48131 \AA) > EBHP ($\text{HO}-\text{O}-\text{CHCH}_3$, 1.48002 \AA) > toluene hydroperoxide ($\text{HO}-\text{O}-\text{CH}_2-$, 1.47663 \AA), thus the most O–O bond length is probably the most susceptible to radical-induced decomposition resulting in a lower concentration. In contrast, the high stabilization of hydroperoxide such as EBHP can maintain the high level of oxygen transfer efficiency, which is consistent with the high epoxide selectivity for ethylbenzene as solvents. To find additional support, we also subject cyclohexene to epoxidation with molecular oxygen in DMSO that has previously been employed in the aerobic epoxidation of cyclohexene (entry 18). No conversion of cyclohexene to its oxide, however, were detected, which may be attributed to the good fact that DMSO without containing the alkyl C–H bond can not be activated for hydroperoxide intermediates by O_2 in the epoxidation reaction. In

addition, our investigations seen in Table 3 with substrates such as cycloheptene and 1-octene, in the presence of ethylbenzene as a solvent also give rise to the good epoxide selectivity (51% and 98%).

The synergistic studies show that the observed reactivity is consistent with an EBHP as key oxygen transfer intermediate whose fate ultimately dictates the epoxide product selectivity. We further explore various factors that control selectivities in α -C–H bond oxidation or deep-oxidation versus C=C bond epoxidation of cyclohexene under the CoMo heterogeneous catalysis. Fig. 6A shows that the cyclohexene/ethylbenzene mass ratio has an obvious influence on the reaction pathway. It is well observed that the conversion of cyclohexene decreases initially and then increases rapidly, but epoxide selectivity increases initially and then decreases with increasing cyclohexene/ethylbenzene mass ratio. A possible explanation for this phenomenon is a high or low concentration of EBHP obtained in reaction system is not beneficial for oxygen transfer process to make the epoxide, resulting in a α -C–H bond oxidation of cyclohexene or radical polymerization to form large number of undesired products. Results of product selectivity let us to conclude that an optimum cyclohexene/ethylbenzene mass ratio of 1.5:8 can be controlled in which the epoxide yields are maximized, indicating that the formation of allylic hydroperoxides from cyclohexene with α -C–H bond oxidation or radical polymerization is avoided in a large extent.

The effect of the temperature on the C=C bond epoxidation of cyclohexene conversion is investigated and plotted in Fig. 6B. At temperatures lower than 70°C , no conversion of cyclohexene and ethylbenzene to its peroxide is observed, respectively (not shown). As shown in Fig. 6B, the effect of the reaction temperature ($> 110^\circ\text{C}$) on the cyclohexene conversion and the epoxide selectivity is very strong. Cyclohexene conversion increases from 11.4% to 62.5%, but epoxide selectivity increases initially and then decreases with increasing reaction temperature from 110 to 150°C . These results indicate that a higher reaction energy (higher temperature) favors the occurrence of oxygen transfer by direct C=C bond epoxidation of cyclohexene as well as easy production of EBHP through a radical way, avoiding the non-catalytic EBHP decomposition and cyclohexene self-oxidation. Further increasing the temperature from 130 to 150°C results in a decrease in the epoxide selectivity from 59.1% to 40%, which may be attributed to rapid radical polymerization or hydrolysis of epoxide production.

Fig. 6C shows the effect of reaction time on both cyclohexene conversion and selectivity to epoxide. It is well noted that with increasing time, initially the epoxide selectivity (till 60 min) changes slightly, but after 60 min the epoxide selectivity decreases very rapidly. In the meantime, it is also found that the cyclohexene conversion always increases. A possible explanation for this phenomenon is a radical-type solvent peroxidation process. In order to find out the EBHP intermediates, we take aliquots of the sample at regular intervals and analyses them by iodometric titration. EBHP concentration almost keeps at a constant level with the reaction time, which indicates that these EBHP intermediates are effectively mediate the first step of the overall oxidation cycle with oxygen transfer to yield epoxide products. Further increasing the reaction time causes the decline of epoxide yield, implying occurrence of epoxide polymerization via formation of non-detected products (by GC-MS). This phenomenon is quite consistent with the results obtained by Neumann et al., implying that short reaction times is critical to obtain high epoxide selectivity [53]. Fig. 6D presents that with increasing reaction pressure, the epoxide selectivity almost keeps at a constant level initially and decreases after $> 0.6 \text{ MPa}$. This is due to the fact that high pressure can enhance oxygen solubility making more oxygen molecules accessible in the reaction medium. Thus, epoxide and cyclohexene self-oxidation occur easily at the same time.

The recyclability test for hollow CoMo bimetallic oxide (2:1) is performed at 130°C and 0.6 MPa oxygen pressure. After simple separation and pretreatment, hollow CoMo bimetallic oxide still can maintain its catalytic activity (30%) and epoxide selectivity slightly

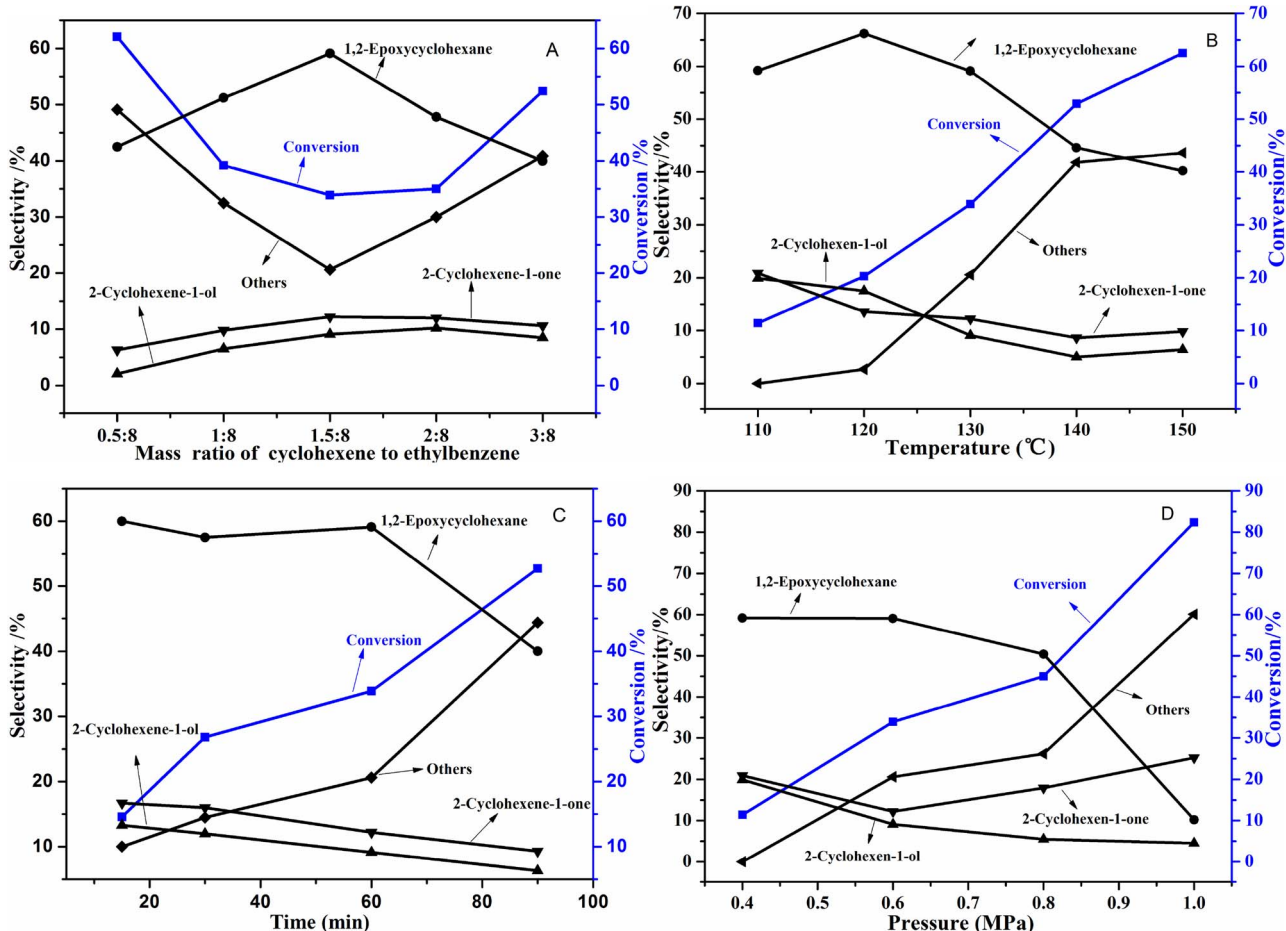


Fig. 6. Effect of the mole ratio of cyclohexene to ethylbenzene (A), temperature (B), reaction time (C) and pressure (D) on the conversion of cyclohexene and 1, 2-epoxycyclohexane, 2-cyclohexen-1-ol, 2-cyclohexen-1-one and others selectivity over the synthesized hollow CoMo bimetallic catalysts.

decreases for five successive oxidation cycles (Fig. 7), demonstrating its good recyclability and deactivation resistance. Meanwhile, after completion of the fifth test reaction, the solid oxide is separated from the reaction mixture by hot-filtration and the resulting filtrate is independently analyzed by ICP-AES analysis. It is found that Co or Mo ions are hardly detected in the filtrate, which is further proved to be truly of a heterogeneous nature. As a result, its excellent synergistic

catalysis and recyclability will make this cheap bimetallic oxide attractive for both fundamental research and practical applications.

4. Discussion

4.1. Reactivities and structure of active species

In the above sections, the high activity of hollow CoMo bimetallic catalysts for aerobic epoxidation of cyclohexene containing labile allylic hydrogen atoms has been rarely observed for monometallic Co_3O_4 or MoO_3 , which is attributed to the hollow CoMo bimetallic synergistic catalysis in the oxygen transfer process. To understand the reactivities and structure of active species for synergistic catalysis, we examined the aerobic oxidation of pure cyclohexene and ethylbenzene by using the Co_3O_4 catalyst under similar conditions. The Co_3O_4 catalyst exhibits the high activity of $\alpha\text{-C}=\text{H}$ bond oxidation with very poor selectivity to epoxide (22%) for aerobic epoxidation of cyclohexene at 80 °C and shows the high ethylbenzene peroxidation conversion (4%, see Table 3). From the structural analysis, it is known that the surface of the Co_3O_4 is terminated by the cobalt (II) sites. Thus, these cobalt (II) sites in the presence of oxygen vacancies can bind and activate oxygen-forming $\text{Co}(\text{III})-(\text{O}_2^-)$ species, and further undergo reaction to yield peroxy or superoxo radical-type active oxygens for nonselective $\alpha\text{-C}-\text{H}$ bond of cyclohexene oxidation or further deep-oxidation [13]. This is quite similar to the interpretation of the cobalt (II) sites for ethylbenzene peroxidation, in which surface $\text{Co}(\text{III})-(\text{O}^{2-})$ species activate O_2 to form EBHP. On the other hand, the large positive charge of the molybdenum (VI) sites is capable of accepting electron pairs in vacant d orbitals, making them excellent catalysts for epoxidation reactions

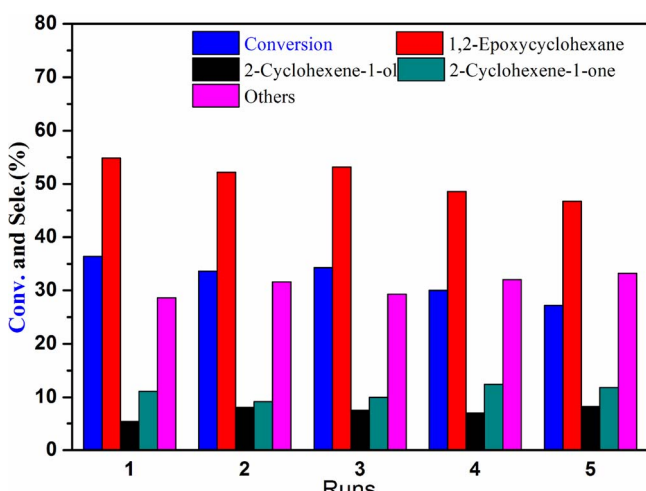


Fig. 7. Recyclability tests of Co/Mo = 2:1 catalyst for the cyclohexene epoxidation. All reactions were carried out with 0.20 g of catalyst, 1.5 g cyclohexene, 8.0 g of ethylbenzene, 0.6 MPa O_2 , 130 °C, time (1 h).

[16]. In various respects the epoxidation behavior of molybdenum (VI) species with EBHP as oxygen sources is, however, very different from Ti species. One of the unique features is the outstanding geometric and electronic structure dependency of the activity of molybdenum (VI) species [54]. For example, $[\text{MoO}_2(\text{inime})(\text{L})]$ bearing different axial ligands ($-\text{N}_3$, $-\text{Cl}$, $-\mu\text{-O}$) is studied in the epoxidation of alkenes and observed a different reactivity [55]. These results indicate that an increase in the nucleophilicity of the Mo(VI)-peroxy unit upon binding of anionic axial ligands makes its more reactive in oxidative nucleophilic reactions. In addition, the immobilization of Mo(VI) species onto inorganic or organic solids has been tested in the epoxidation of alkenes with EBHP as an oxidant, and structure-activity relation of the catalyst are also revealed [56]. Compared with the excellent $\alpha\text{-C-H}$ bond oxidation activity of the Co_3O_4 in aerobic oxidation, its low activity in epoxidation demonstrates that the single Mo(VI) species do not efficiently activate dioxygen for direct cyclohexene epoxidation. The absence of EBHP as oxygen transfer reagents for the next the $\text{C}=\text{C}$ bond epoxidation may be another reason for the inferior activity.

We have found that the hollow bimetallic CoMo catalyst with a lower Co/Mo mole ratio (1:3) calcined at 500 °C shows a favorable catalytic epoxidation activity with the epoxide selectivity of 65.7% at a cyclohexene conversion of 11.3%. Analyses of product distribution reveal that the presence of Co^{2+} species increases epoxidation rate. It is clearly demonstrated that the route of $\text{C}=\text{C}$ bond epoxidation can be enhanced by modification with Co^{2+} species. As shown in characterization results, the hollow bimetallic CoMo catalysts present a XRD peak at $2\theta = 23.6^\circ$ that is typical for CoMoO_4 -like structure (Fig. 1). The oxides are physically mixed with pure MoO_3 and Co_3O_4 without particular interactions (FT-IR and Raman, Fig. 3), which is the low selectivity to epoxide. The CoMoO_4 -like species (octahedral $[\text{MoO}_6]$) for this hollow bimetallic CoMo oxide, composed of $\text{Mo}-\text{O}-\text{Co}$ unit or that of $\text{Mo}-\text{O}^{\delta-}\cdots\text{Co}^{\delta+}$ at least, is also confirmed by Raman and FT-IR observations. These $\text{Mo}-\text{O}-\text{Co}$ and/or $\text{Mo}-\text{O}^{\delta-}\cdots\text{Co}^{\delta+}$ unit are supposed to be active centers for cyclohexene epoxidation and ethylbenzene peroxidation because most cyclohexene converted and epoxide yield is the higher compared with the physical mixture of MoO_3 and Co_3O_4 . In addition, isolate MoO_3 crystallites are identified, particularly, dissociation of the structure of MoO_3 takes place greatly, accompanying with the evolution of local octahedral coordination (MoO_6) to tetrahedral one (MoO_4) (Fig. 4). For the Co-modified CoMo oxide series of catalysts, the synthetic effect of Co on cyclohexene conversion becomes evident with the increase of the Co/Mo molar ratios. Characterizations of catalysts using XRD and TEM suggest that increasing Co/Mo molar ratios to 2:1 induces continuous (crystal) structure changes of CoMoO_4 -like and MoO_3 species in the catalysts. The MoO_3 species observed in sample with Co/Mo mole ratio of 2:1 disappear and are gradually replaced by a number of complicated hetero-polyoxo-Mo/Co agglomerates, such as CoMoO_4 -like and Co_3O_4 species. Meanwhile, the tetrahedral MoO_4 species, come from the dissociation of MoO_3 crystal, evolve to CoMoO_4 -like forms. In addition, the evolution of apparent $\text{Co}-\text{O}-\text{Mo}$ peaks suggests that more Co species may bond to Mo atoms on MoO_3 surface through $\text{Co}-\text{O}-\text{Mo}$ interaction. These interactions between hetero-polyoxo-Mo/Co agglomerate and Co_3O_4 species are proposed to suppress the reactivity of the lattice oxygen species associated with the Co_3O_4 crystal, which is generally regarded as nucleophilic oxygen species leading to the allylic oxidation or further deep-oxidation. Further increasing Co/Mo molar ratios to 3:1 indicates that Co_3O_4 species is gradually enriched on the surface and ultimately leads to complete Co_3O_4 crystal phase segregation with the disappearance of hollow structure, resulting in the low epoxide selectivity. This may be attributed to the disappearance of highly active species, such as hetero-polyoxo-Mo/Co agglomerate, and O atom of EBHP cannot transfer to cyclohexene efficiently. Based on the results and discussion above, the structure of the different catalysts is proposed in our catalytic systems (Fig. 8). As a result, Mo(VI) species in hollow bimetallic CoMo oxide having unique geometric and electronic structure favor the $\text{C}=\text{C}$ bond

epoxidation by oxygen transfer process, as similarly observed in homogeneous Mo(VI) complex-based catalytic system.

4.2. Density functional theory treatments of oxygen activation and oxygen atom transfer

On the basis of experimental examination of surface species by Raman, XPS, UV-vis and FT-IR methods, in theoretical studies we imagine the smallest structural model CoMoO_4 containing two different active sites (Co sites and Mo sites). This is a highly simplified system, and DFT calculations are carried out only to elucidate the electronic distribution and band patterns of active structures. Fig. 9A shows the NBO charge on the metal sites in the optimized CoMoO_4 structure scales with their formal valence state (Co^{2+} , Mo^{6+}). The Co sites expose the small positive charge (+0.925 e), whereas the larger (+1.482 e) charge characterizes the Mo sites. Since the NBO charge accumulated on the central metal can be the measure of the electrophilicity of an active center, the performed calculations indicate that the electrophilic feature of Mo sites is much stronger toward the $\text{C}=\text{C}$ bond bearing a partial negative charge than that Co sites among the studied catalyst.

To get insight about how the hollow CoMo bimetallic catalysts can activate oxygen, the interactions between O_2 and the Co or Mo sites in Figs. 9C and D are investigated, respectively. Initially, the metal site is fixed and an oxygen molecule is placed nearby and optimized by periodic DFT calculations. Figs. 9C and D show that O_2 can be bonded to Co sites with starting from initial configuration, whereas the O_2 always lefts the Mo sites. This suggests that the activation of molecular oxygen easily occurs on the Co sites by partial electron transfer from the Co site to the $2\pi^*$ anti-bonding orbital of O_2 [57]. Interestingly, the O–O bond length of (c) is elongated after adsorption from 1.2128 Å (free O_2 , experimental $d_{\text{O}-\text{O}}$) to 1.2305 Å, showing a typical value of the superoxo- Co^{3+} fragment found in other literature examples [23,58]. However, the O–O distance (1.2133 Å) for (d) absorption model is kept nearly constant throughout the calculation; only the atomic positions are allowed to relax. This can be explained by the following fact: the increase of the O–O bond lengths is correlated with the formation of the metal–oxygen bond, resulting from the orbital overlap between inplane $\text{O}_2 \pi^*$ orbital and Co d_{xy} orbital. Further, a NBO charge analysis is performed to investigate the charge distribution. Upon adsorption, the NBO charge of Co atom is increased from 0.925 e to 1.044 e, which indicates that a partial charge transfer occurs from the Co electronic back-donation to O_2 . In contrast, there is a small charge transfer of 0.057 e from Mo to the oxygen molecule, which also suggests that there is no sign of a more pronounced activation of the O_2 when this interacts with Co sites compared to Mo sites. Besides, we have quantified the activation of molecule oxygen on the different metal active sites by looking at the O–O stretching frequencies in the $\text{Co}-\text{O}_2$ (1471 cm⁻¹) and $\text{Mo}-\text{O}_2$ (1657 cm⁻¹) complexes (Fig. 10). In line with the above results, a significant decrease in the O–O stretching frequency provides a clear indication of O_2 activation in the case of Co sites [59]. Additionally, the coordinated oxygen atom in the $\text{Co}-\text{O}_2$ complex bears a higher negative charge (-0.1431e) compared with the distal oxygen atom (0.1090 e), as shown in Fig. 9C. Thus, from the above discussion, we conclude that a homolytic cleavage of the weak C–H bond of ethylbenzene occurs easily over the coordinated oxygen atom with a higher negative charge in the $\text{Co}-\text{O}_2$ complex to form phenylethyl radicals and thus benefiting the catalytic performance.

As noted above, the catalytic epoxidation probably occurs on the Mo site of the catalyst. In order to better understand the effect of activation or deactivation at the peroxy center by the metal Mo with oxygen atom transfer, one peroxy group is introduced into the system, and the overall structure shown in Fig. 9B is fully optimized. Fig. 9B displays that the O–O bond length is significantly elongated from 1.3921 Å (as calculated in free organic peroxyde at the same level) to 1.4454 Å, which indicates an activation of the peroxy group by the Mo metal center, resulting in a lower reaction energy barrier. While for Co

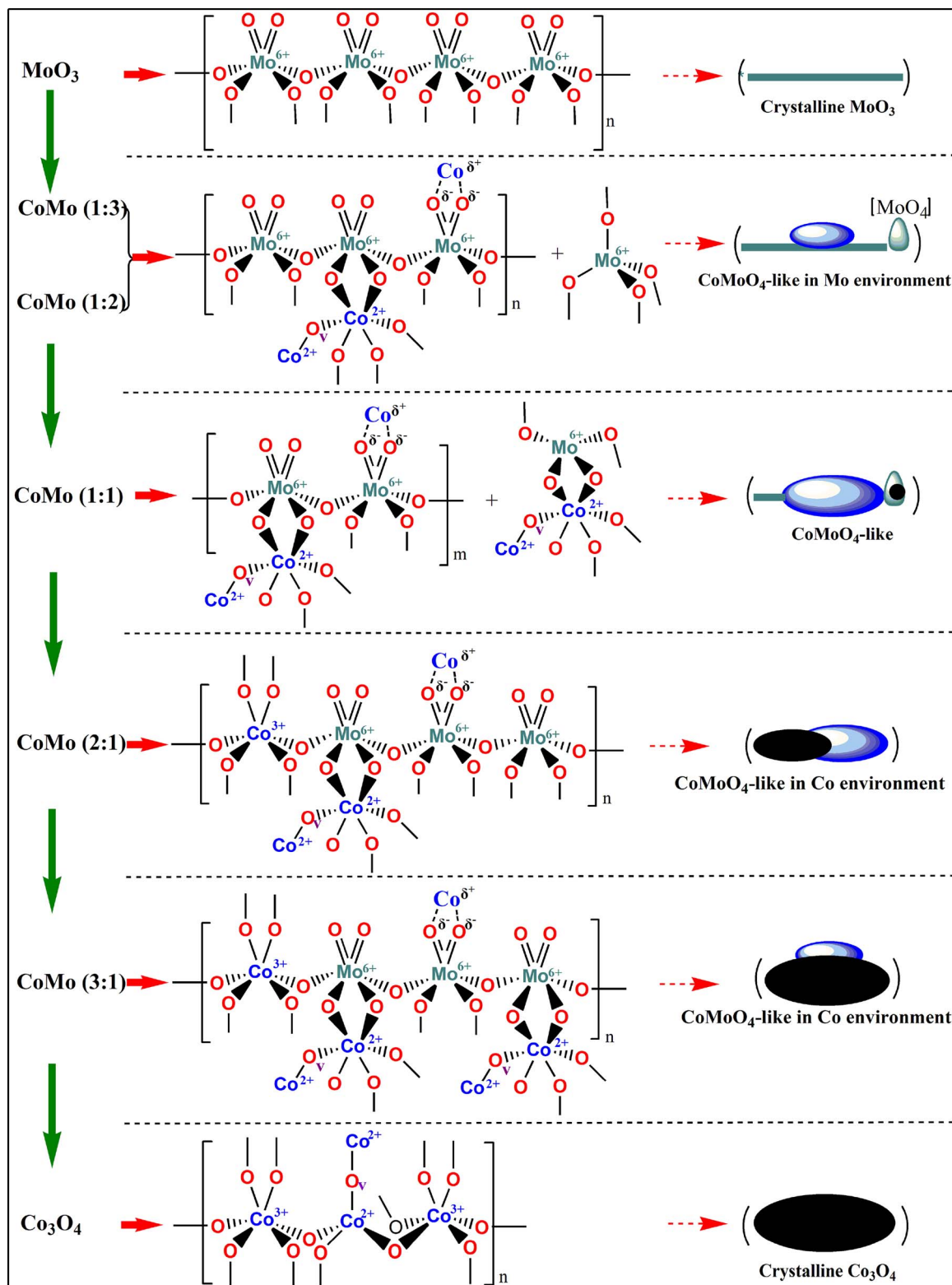


Fig. 8. Schematic description of the structure of the different CoMo catalysts, as derived from the characterization methods.

peroxide the O–O distance is calculated noticeably shorter than organic peroxide (not shown), by about 0.05 Å, indicative of a deactivation of the peroxy group. Further, the oxygen centers of peroxy group are not equivalent as can be seen from the distances $\text{Mo}-\text{O}_{\text{left}}$, 1.9568 Å and $\text{Mo}-\text{O}_{\text{right}}$, 1.9036 Å; the oxygen center O_{left} exhibits a larger negative charge (0.310 e) than the oxygen center O_{right} (0.296e). The reason for the structural asymmetry of the metalperoxy group and concomitant

charge distribution can be related to orbital overlap by the $\pi^*(\text{O}-\text{O})$ and $d(\text{M})$ orbitals. On the basis of previous investigations [60], the epoxidation reaction is described as a $\text{S}_{\text{N}2}$ -like process in which a nucleophilic cyclohexene is attacked by an electrophilic peroxy compounds. In our catalytic system, the electrophilic character of the oxygen transfer (O_{right} with a smaller negative charge) is significantly manifested through the electron density transfer in the cyclohexene-

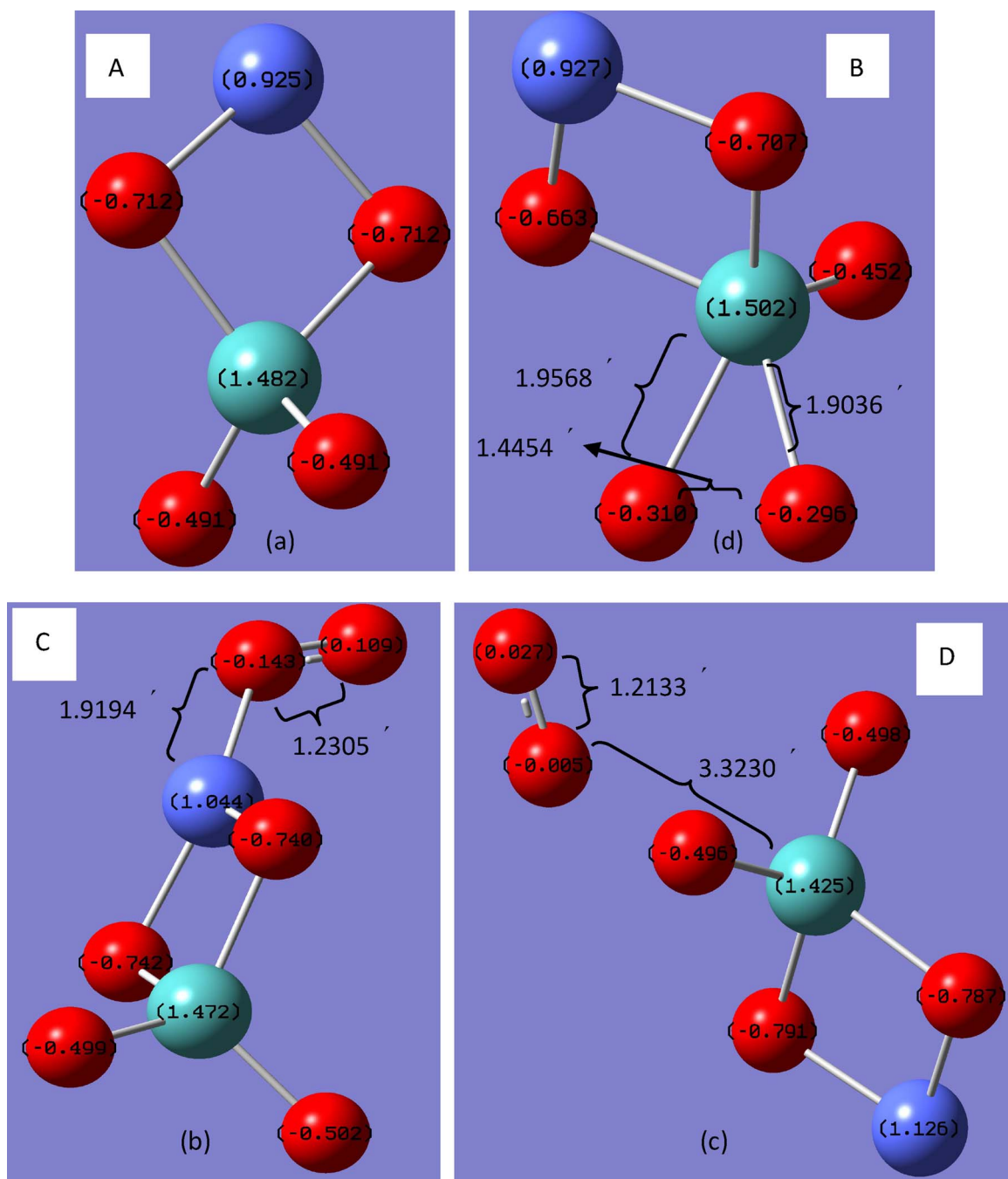


Fig. 9. Suggested simple models and electronic structure of optimized models for the CoMoO₄ (a), CoMoO₄ with the interactions between O₂ and the Co sites (b) or Mo sites (c), and CoMoO₄ with the Mo-peroxo groups.

peroxo-Mo transition state from absorbed cyclohexene to the peroxy-Mo complex. In fact, such electron density transfer results from the interaction of the π (C-C) HOMO of cyclohexene and the unoccupied O–O antibonding orbital $\delta^*(\text{O–O})$ of the peroxy complex, which is easy for homolytic cleavage of the longer O–O bond of peroxy complex for oxygen atom transfer to cyclohexene.

4.3. Synergistic effect and reaction pathways

On the basis of the above experimental and computational studies, an illustration of possible synergistic effect behavior and the corresponding pathways for the aerobic oxidation of cyclohexene to epoxide over the hollow CoMo bimetallic catalysts may occur through two oxygen transfer processes (**Scheme 2**). They are (i) the Co²⁺-catalyzed

peroxidation of solvents to form an electrophilic oxygen species such as O₂[–] or OOH, (ii) subsequent molybdenum-catalyzed epoxidation of cyclohexene. For the first one, the activation and dissociation of molecular oxygen have been accomplished by using Co²⁺ sites as the main active participants in the catalytic cycle. This supports by the findings: (i) the facile electronic density transfer to antibonding orbitals with lengthening the O–O bond by DFT, (ii) facile Co²⁺ → Co³⁺ oxidation by heating in O₂, and (iii) inferior activity of Co₃O₄ free metal catalyst for cyclohexene or ethylbenzene oxidation. In addition, previous reports obtained important evidence also suggest that Co species are capable of activating O₂ [61–63]. Further, it is worth noting that our results show that the resulting additional oxygen vacancies by creation and stabilization of Mo⁶⁺ site may be involved in O₂ activation. Taking into account the catalytic experiments and all the evidence that the

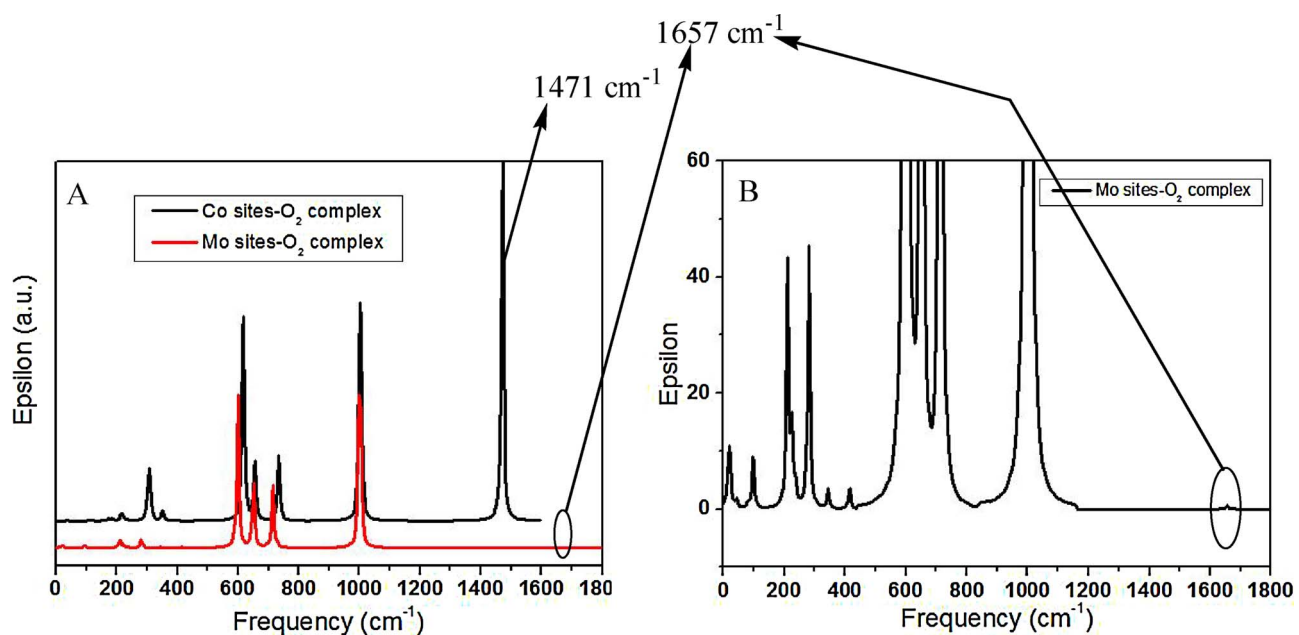
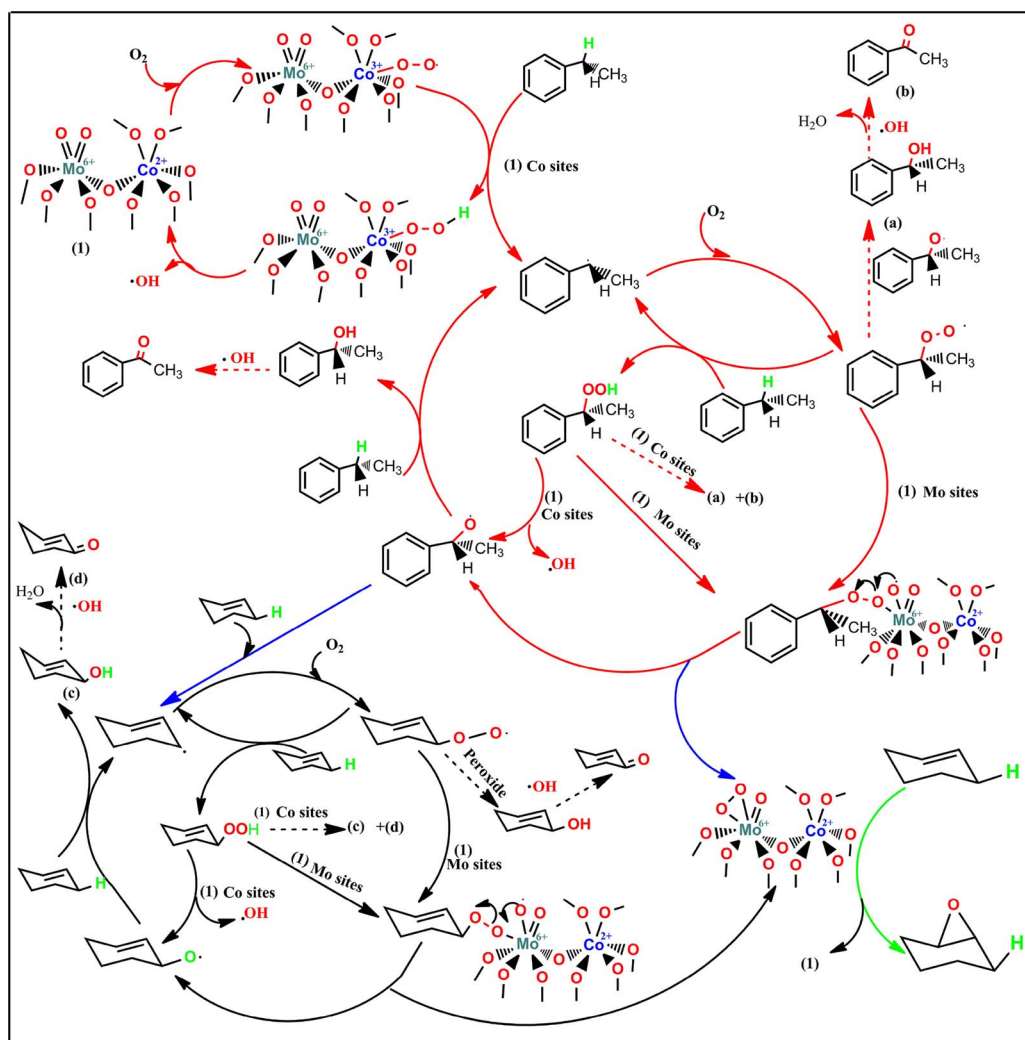


Fig. 10. Computational FT-IR spectra for the optimized CoMoO₄ with the interactions between O₂ and the Co sites or Mo sites.



Scheme 2. Mechanistic pathway for aerobic epoxidation of cyclohexene to 1, 2-epoxycyclohexane.

intermediates are detected, we propose that the possible per-oxidation pathway with the first oxygen transfer process for Co sites catalyzed aerobic solvent oxidation is as follows: initially, O_2 is activated on a reduced metal Co^{2+} sites in the $Mo-O-Co$ and/or $Mo-O^{\delta-}...Co^{\delta+}$ unit, resulting in the $Co^{3+}-O_2$ complex [62,64]. The hydrogen atom abstraction from the weakest methylene C–H bond of ethylbenzene but not from cyclohexene by the action of the $Co^{3+}-O_2$ complex generates the active phenylethyl radicals, which is rapidly trapped by O_2 to give a phenylethylperoxy radicals [13]. This phenylethylperoxy radical will preferentially carry out the kinetically-favored addition to cyclohexene instead of H abstraction from ethylbenzene or allylic hydrogen atom of cyclohexene [65]. If this phenylethylperoxy radicals do not add preferentially to cyclohexene, it will be rapidly trapped by another ethylbenzene molecular to give an EBHP on which subsequent decomposition by Co^{2+} sites produces a mixture of alcohol and ketone.

Second, epoxidation of cyclohexene with the above phenylethylperoxy radicals or EBHP is facilitated by Mo^{6+} sites, which is confirmed by the evidences: (i) the larger positive charge of the molybdenum (VI) sites with the formation of stable Mo-peroxy complexes, (ii) the more electrophilicity of the peroxidic distal O atom in Mo-peroxy species and (iii) very high epoxide selectivity of Mo metal catalyst. In addition, recent theoretical and experimental works have determined that the epoxidation of $C=C$ bond with alkyl hydroperoxide on the Mo^{6+} sites is kinetically favorable [66], whereas the formation of allylic radicals on the Mo^{6+} sites is unfavorable. According to our evidence and the description proposed here, the second oxygen transfer process of cyclohexene epoxidation with phenylethylperoxy radical or EBHP over the Mo^{6+} sites of $Mo-O-Co$ and/or $Mo-O^{\delta-}...Co^{\delta+}$ unit will take place between the phenylethylperoxy radical or EBHP adsorbed on the Mo^{6+} sites with the vacant d orbitals and the cyclohexene adsorbed on the same Mo^{6+} sites to give the desired epoxide under the reaction conditions. In this respect, the addition of the radical of the phenylethylperoxy family or EBHP towards a terminal $Mo=O$ group is a lot more active than their phenylethyl radical counterparts to give Mo-peroxy complexes, which will rapidly fragment into Mo-peroxy compound and the propagating alkoxy radical [22,67]. The peroxidic distal O atom in Mo-peroxy species is more electrophilic and, therefore, more likely to be attacked by an electron-rich olefins with pre-coordination to the electron-deficient Mo^{6+} center. Then, distal-oxygen transfer reaction toward the cyclohexene occurs, producing the epoxide and the initial catalytic species (1) [67]. On the other hand, these obtained alkoxy radicals are highly reactive towards H abstraction than their phenylethylperoxy radical counterparts and will abstract one H from ethylbenzene (or cyclohexene) to form 1-phenylethanol and regenerate the propagating phenylethyl radical (or allylic) radical [65]. As a result, 1-phenylethanol should be formed as a main solvent product (main acetophenone is formed by non-selective decomposition in the case of EBHP), as we have also observed in our study. Additionally, the allylic radical of cyclohexene is rapidly trapped by O_2 to give an allylicperoxy radicals, which will be transformed to 3-hydroperoxycyclohex-1-ene by kinetically-limited H abstraction on its parent molecule. Autoxidation of allylic hydrogen of cyclohexene then relies on the decomposition of this hydroperoxide to allylic oxidation products by the Co^{2+} sites, since the process of cyclohexene epoxidation with allylic hydroperoxide over the Mo^{6+} sites may also occur [4]. In our system, it is clearly demonstrated that the route of α -C–H bond autoxidation may be suppressed by $Mo-O-Co$ and/or $Mo-O^{\delta-}...Co^{\delta+}$ unit, which is consistent with the changes in epoxide selectivity (the observed structural evolution of catalytic species). In addition, the above formed alcohols can be further oxidized with the production of $\cdot OH$ at the weakest methine C–H bond (~ 96 kcal/mol) to form geminal diol intermediates, which is well-known to be very unstable and will rapidly undergo dehydration to product stable ketones [68,65]. Actually, the side reaction mechanism for $\cdot OH$ radical-mediated oxidative conversion of alcohol to ketone is supported by reaction intermediates detection during the reaction time course.

Hydrolysis and polymerization of the epoxide are also negligible side reactions.

Finally, it is clear that in Co^{2+} species of CoMo bimetallic catalysts two effects cooperate for the observed improvement of the cyclohexene epoxidation ability through oxygen transfer processes: (i) the creation and stabilization of additional oxygen vacancies by Mo^{6+} site to enhance absorption and activation of O_2 , and (ii) the promotion of the electronic transfer between the Co^{2+} and Mo^{6+} species. The synergistic effects can be obtained in terms of the characterization results, because, higher the population of oxygen vacancies and higher the possibility for such electronic transfer in $Mo = O...Co^{2+} - O_v - Co^{2+} + O_2 \rightarrow [Mo = O...Co^{3+} - O_v - Co^{3+})O_2^-]$ process. In fact, for the enhancement of oxygen activity on transition metal oxide, the most common method to meet this subject has also been choose a suitable doping cation for aerobic oxidation [69,70]. In our works, the creation of oxygen vacancies by the interaction of the Co_3O_4 species and the Mo^{6+} species is commonly proposed as a determinant structural effect that facilitates the adsorption and activation of molecule oxygen for ethylbenzene peroxidation reaction. On the other hand, it is clearly demonstrated that the route of α -C–H bond autoxidation may be suppressed by interaction of the Co_3O_4 species and the Mo^{6+} species. In good agreement with our results, the enhancement of $C=C$ bond epoxidation by the promotion of electronic transfer between Co^{2+} species and doping agent (or complex) can be observed in other systems also applied for the alkene epoxidation reaction. Therefore, we speculate that the promotion of the electronic transfer between the Co^{2+} species and Mo^{6+} can inhibit the allylic oxidation route to the formation of allylic oxidation products and enhance the catalytic performance for epoxidation of cyclohexene to form 1,2-epoxycyclohexane.

5. Conclusion

The hollow-structured CoMo bimetallic catalysts engineered from micro- to macro-scale are developed for the direct aerobic epoxidation of cyclohexene containing labile allylic hydrogen atoms to the corresponding epoxides, providing unique combination of high activity/selectivity toward the $C=C$ bond epoxidation and good stability. The results, obtained from the comprehensive experimental studies involving the characterization, detection, reaction of the different alkenes, reactions conditions, as well as computational investigations, have demonstrated that the surface Co^{2+} species in octahedrally coordinated environment are responsible for the first step of the O_2 activation that convert O_2 into $Co^{3+}-O_2$ complex and further involve the formation of EBHP, while the subsequent oxygen atom transfer step of EBHP to cyclohexene is catalyzed by Mo sites. Further, the hollow-structured CoMo bimetallic catalysts show the higher epoxidation performances than the physical mixture of MoO_3 and Co_3O_4 . The remarkably different catalytic behavior suggests that the relative rates of the $C=C$ bond epoxidation (leading to epoxides) versus α -C–H bond oxidation (leading to allylic oxidation products) can be controlled by the expansion of unit cell, structural defects and modified the electronic structure of $CoMoO_4$ by the presence of Co_3O_4 species on the surface of the catalysts. With an optimized Co/Mo mole ratio of 2:1, a high 1,2-epoxycyclohexane selectivity of 59% at 33% cyclohexene conversion has been obtained. The tunability of hollow-structured CoMo catalysts will allow one to apply for impoving the efficiency of existing traditional “hydroperoxide” process based on intermolecular heterogeneous catalysis.

Acknowledgments

This work was supported by the Natural Science Foundation of China (Grant No.21576078 and 21776068) and the Natural Science Foundation of Hunan Province (Grant No.2016JJ2081) and Innovation Platform Open Fund of Hunan College (16K052) and Collaborative Innovation Center of New Chemical Technologies for Environmental Benignity and Efficient Resource Utilization.

References

- [1] S. Caron, R.W. Dugger, S.G. Ruggeri, J.A. Ragan, D.H.B. Ripin, *Chem. Rev.* 106 (2006) 2943–2989.
- [2] J. Dou, F. (Feng) Tao, *Appl. Catal. A: Gen.* 529 (2017) 134–142.
- [3] J. García-Aguilar, I. Miguel-García, J. Juan-Juan, I. Such-Basáñez, E.S. Fabián, D. Cazorla-Amorós, Á. Berenguer-Murcia, *J. Catal.* 338 (2016) 154–167.
- [4] B.P.C. Hereijgers, R.F. Parton, B.M. Weckhuysen, *Catal. Sci. Technol.* 2 (2012) 951–960.
- [5] J. Tsuji, J. Yamamoto, A. Corma, F. Rey, 1998, U.S. Patent, 6, 211, 388.
- [6] M.T. Navarro, A. Corma, J.L. Jordà, F. Rey, 2000, WO 2000007710 A2.
- [7] E.E. Chufán, S.C. Puiu, K.D. Karlin, *Acc. Chem. Res.* 40 (2007) 563–572.
- [8] X. Feng, X. Duan, G. Qian, X. Zhou, D. Chen, W. Yuan, *Appl. Catal. B: Environ.* 150–151 (2014) 396–401.
- [9] I. Yamanaka, K. Nakagaki, K. Otsuka, *J. Chem. Soc. Chem. Commun.* 11 (1995) 1185–1186.
- [10] I. Iwahama, G. Hatta, S. Sakaguchi, Y. Ishii, *Chem. Commun.* 2 (2000) 163–164.
- [11] J. Sebastian, K.M. Jinka, R.V. Jasra, *J. Catal.* 244 (2006) 208–218.
- [12] L. Hu, L. Shi, H. Hong, M. Li, Q. Bao, J. Tang, J. Ge, J. Lu, X. Cao, H. Gu, *Chem. Commun.* 46 (2010) 8591–8593.
- [13] R.A. Sheldon, J.K. Kochi, *Metal-Catalysed Oxidation of Organic Compounds*, Academic Press, New York, 1981.
- [14] M.J. da Silva, P. Robles-Duthefner, L. Menini, E.V. Gusevskaya, *J. Mol. Catal. A Chem.* 201 (2003) 71–77.
- [15] B. Rhodes, S. Rowling, P. Tidswell, S. Woodward, S.M. Brown, *J. Mol. Catal. A Chem.* 116 (1997) 375–384.
- [16] F.E. Kühn, A.M. Santos, M. Abrantes, *Chem. Rev.* 106 (2006) 2455–2475.
- [17] R.A. Sheldon, J.A. Van Doorn, *J. Catal.* 31 (1973) 427–437.
- [18] F.E. Kühn, W.-M. Xue, A. Al-Ajlouni, A.M. Santos, S. Zang, C.C. Romão, G. Eickerling, E. Herdtweck, *Inorg. Chem.* 41 (2002) 4468–4477.
- [19] F.E. Kühn, E. Herdtweck, J.J. Haider, W.A. Herrmann, I.S. Gonçalves, A.D. Lopes, C.C. Romão, *J. Organomet. Chem.* 583 (1999) 3–10.
- [20] Y.S. Yoon, N. Fujikawa, W. Ueda, Y. Moro-oka, W. Lee, *Catal. Today* 24 (1995) 327–333.
- [21] C.D. Valentin, P. Gisdakis, I.V. Yudanov, N. Rösch, *J. Org. Chem.* 65 (2000) 2996–3004.
- [22] P. González-Navarrete, F.R. Sensato, J. Andrés, E. Longo, *J. Phys. Chem. A* 118 (2014) 6092–6103.
- [23] D. Rutkowska-Zbik, R. Tokarz-Sobieraj, M. Witko, *J. Chem. Theory Comput.* 3 (2007) 914–920.
- [24] Y. Lei, X. Chen, C. Xu, Z. Dai, K. Wei, *J. Catal.* 321 (2015) 100–112.
- [25] M.I. Fadlalla, H.B. Friedrich, *Catal. Sci. Technol.* 4 (2014) 4378–4385.
- [26] C. Cao, L. Xing, Y. Yang, Y. Tian, T. Ding, J. Zhang, T. Hu, L. Zheng, X. Li, *Appl. Catal. B: Environ.* 218 (2017) 32–45.
- [27] M. Hu, Y. Murakami, M. Ogura, S. Martuyama, T. Okubo, *J. Catal.* 225 (2004) 230–239.
- [28] V.O.O. Goncalves, C. Ciottonea, S. Arri-clacens, N. Guignard, C. Roudaut, J. Rousseau, J.-M. Clacens, S. Royer, F. Richard, *Appl. Catal. B: Environ.* 214 (2017) 57–66.
- [29] J. Vakrosa, A. Lycourghiotis, G.A. Voyatzis, A. Siokou, C. Kordulis, *Appl. Catal. B: Environ.* 96 (2010) 496–507.
- [30] M.C. Cabanas, G. Binotto, D. Larcher, A. Lecup, V. Giordani, J.M. Tarascon, *Chem. Mater.* 21 (2009) 1939–1947.
- [31] D. Meng, Q. Xu, Y. Jiao, Y. Guo, Y. Guo, L. Wang, G. Lu, W. Zhan, *Appl. Catal. B: Environ.* 221 (2018) 652–663.
- [32] G.W. Graham, W.H. Weber, C.R. Peters, R. Usmen, *J. Catal.* 130 (1991) 310–313.
- [33] M.V. Ganduglia-Pirovano, A. Hofmann, J. Sauer, *Surf. Sci. Rep.* 62 (2007) 219–270.
- [34] J.E. Herrera, D.E. Resasco, *J. Phys. Chem. B* 107 (2003) 3738–3746.
- [35] T.A. Zepeda, B. Pawelec, J.L.G. Fierro, A. Montesinos, A. Olivas, S. Fuentes, T. Halachev, *Micropor. Mesopor. Mater.* 111 (2008) 493–506.
- [36] C. Li, Q. Xin, K.-L. Wang, X. Guo, *Appl. Spectrosc.* 45 (1991) 874–882.
- [37] D. Scarano, A. Zecchina, S. Bordiga, F. Geobaldo, G. Spoto, G. Petrini, *J. Chem. Soc. Faraday Trans.* 89 (1993) 4123–4130.
- [38] S.O. Souvi, D. Danset, M.E. Alikhani, L. Manceron, *J. Phys. Chem. A* 114 (2010) 11399–11407.
- [39] A.V. Pashigreva, G.A. Bukhtiyarova, O.V. Klimov, Yu.A. Chesalov, G.S. Litvak, A.S. Noskov, *Catal. Today* 149 (2010) 127–129.
- [40] J.A. Toledo-Antonio, M.A. Cortes-Jacome, J. Escobar-Aguilar, C. Angeles-Chavez, J. Navarrete-Bolanos, E. López-Salinas, *Appl. Catal. B: Environ.* 213 (2017) 106–117.
- [41] L. Peña, D. Valencia, T. Klimova, *Appl. Catal. B: Environ.* 147 (2014) 879–887.
- [42] K. Pearson, R.L. McNaughton, M.L. Kirk, *J. Am. Chem. Soc.* 124 (2002) 9006–9007.
- [43] R. Xu, H.C. Zeng, *Langmuir* 20 (2004) 9780–9790.
- [44] B.M. Weiss, E. Iglesia, *J. Catal.* 272 (2010) 74–81.
- [45] J.E. Herrera, L. Balzano, A. Borgna, W.E. Alvarez, D.E. Resasco, *J. Catal.* 204 (2001) 129–145.
- [46] Ch. Papadopoulou, J. Vakros, H.K. Matralis, Ch. Kordulis, A. Lycourghiotis, *J. Colloid Interf. Sci.* 261 (2003) 146–153.
- [47] L. Ma, C.Y. Seo, X. Chen, K. Sun, J.W. Schwank, *Appl. Catal. B: Environ.* 222 (2018) 44–58.
- [48] R.L. Chin, D.M. Hercules, *J. Phys. Chem.* 86 (1982) 3079–3089.
- [49] M. Oku, K. Hirokawa, *J. Electron Spectrosc. Relat. Phenom.* 8 (1976) 475–481.
- [50] Y.V. Plyuto, I.V. Babich, I.V. Plyuto, A.D. Moulijn, J.A. Langeveld, *Appl. Surf. Sci.* 119 (1997) 11–18.
- [51] V.L. Parola, G. Deganello, A.M. Venezia, *Appl. Catal. A: Gen.* 260 (2004) 237–247.
- [52] E. Giannello, Z. Sojka, M. Che, A. Zecchina, *J. Phys. Chem.* 90 (1986) 6084–6091.
- [53] G. Maayan, R. Neumann, *Chem. Commun.* 36 (2005) 4595–4597.
- [54] H. Mimoun, *Angew. Chem. Int. Ed. Engl.* 21 (1982) 734–750.
- [55] J.M. Mitchell, N.S. Finney, *J. Am. Chem. Soc.* 123 (2001) 862–869.
- [56] M.M. Miller, D.C. Sherrington, *J. Catal.* 152 (1995) 368–376.
- [57] A.R. Corcos, O. Villanueva, R.C. Walroth, S.K. Sharma, J. Bacsa, K.M. Lancaster, C.E. MacBeth, J.F. Berry, *J. Am. Chem. Soc.* 138 (2016) 1796–1799.
- [58] E.D. Bloch, L.J. Murray, W.L. Queen, S. Chavan, S.N. Maximoff, J.P. Bigi, R. Krishna, V.K. Peterson, F. Grandjean, G.J. Long, B. Smit, S. Bordiga, C.M. Brown, J.R. Long, *J. Am. Chem. Soc.* 133 (2011) 14814–14822.
- [59] K.J. Naresh, K.R.S. Chandrakumar, K.G. Swapan, *J. Phys. Chem. Lett.* 2 (2011) 1476–1480.
- [60] K.N. Houk, J. Liu, N. DeMello, K.R. Condroski, *J. Am. Chem. Soc.* 119 (1997) 10147–10152.
- [61] W.-Y. Zhou, P. Tian, F. Sun, M.-Y. He, Q. Chen, *J. Catal.* 335 (2016) 105–116.
- [62] T. Hara, T. Iwahama, S. Sakaguchi, Y. Ishii, *J. Org. Chem.* 66 (2001) 6425–6431.
- [63] J. González-Prior, R. López-Fonseca, J.I. Gutiérrez-Ortíz, B. de Rivas, *Appl. Catal. B: Environ.* 222 (2018) 9–17.
- [64] Q. Tang, Q. Zhang, H. Wu, Y. Wang, *J. Catal.* 230 (2005) 384–397.
- [65] J.A. Howard, J.H.B. Chenier, D.A. Holden, *Can. J. Chem.* 56 (1978) 170–175.
- [66] J.M. Mitchell, N.S. Finney, *J. Am. Chem. Soc.* 123 (2001) 862–869.
- [67] A.M. Al-Ajlouni, D. Veljanovski, A. Capapé, J. Zhao, E. Herdtweck, M.J. Calhorda, F.E. Kühn, *Organometallics* 28 (2009) 639–645.
- [68] J. Dai, W. Zhong, W. Yi, M. Liu, L. Mao, Q. Xu, D. Yin, *Appl. Catal. B: Environ.* 192 (2016) 325–341.
- [69] O.H. Laguna, A. Perez, M.A. Centeno, J.A. Odriozola, *Appl. Catal. B: Environ.* 176–177 (2015) 385–395.
- [70] W. Zhong, T. Qiao, J. Dai, L. Mao, Q. Xu, G. Zou, X. Liu, D. Yin, F. Zhao, *J. Catal.* 330 (2015) 208–221.